THE MESOTRON COMPONENT IN COSMIC RAYS

A Study of The Absorption of Mesotrons and An Evaluation of The Mesotron Lifetime

by

Vernal Josephson, B.S., M.S.

A Thesis submitted to the Faculty of Graduate Studies and Research of McGill University in partial fulfillment of the requirements for the degree of Doctor of Philosophy

Macdonald Physics Laboratory

McGill University

April 1942

ACKNOWLEDGEMENTS

The writer wishes to express his sincere appreciation to Drs. D. K. Froman and W. H. Watson, co-directors of this research , for the valuable aid given in this work-- to Dr. Froman for suggesting the problem and the method of solution, and to Dr. Watson for invaluable advice in explaining the results obtained and in preparing this paper. He also wishes to thank Dr. A. N. Shaw, Director of The Macdonald Physics Laboratory for his friendly interest throughout the period of time when the research was carried on.

TABLE OF CONTENTS

SUMMARY

1. A set of Geiger-Muller counters has been manufactured and processed by a method designed to allow them to be operated over a wide voltage plateau from 1200 to 1800 volts.

2. These counters have been used in a triple-quadruple coincidence circuit to obtain the absorption curve for Mesotrons over an absorber range from 1.5 cm to 22.5 cm of Lead. A special arrangement of the counters made it possible to differentiate between the Mesotrons, and the electrons not absorbed by the Lead absorber. The counters were arranged so that all electrons produced quadruple coincidences by producing showers in a Lead shower block, while the Mesotrons produced only triple coincidences. The Mesotron intensity was determined by subtracting the quadruple counts from the triple counts.

3. The rest lifetime of the Mesotron, $\tau_o = 1.63 \pm 0.04$ micro-seconds, has been determined from the shape of the Mesotron momentum spectrum.

4. It is shown that for Mesotrons, the range at sea level in an absorber is a linear function of the momentum range at the point of origin.

5. The results indicate that Mesotrons with a range at sea level up to 10 cm of Lead are produced at a height

of approximately 24 km, while Mesotrons with greater range are produced at lower altitudes. This indication is compatible with results obtained by Hall, and by Regener in recent experiments which they carried out on Mount Evans.

6. It is suggested that the lifetime of the Mesotron can be determined from measurements of the ratio of the number of Mesotrons to the number of disintegration electrons at a given range at different altitudes.

INTRODUCTION

Knowledge of Cosmic Rays dates back to the early days of research in radioactivity. As in all fields of research the collection of accurate information about Cosmic Rays has been slow. This has been due, especially in the earlier period, to the lack of apparatus capable of obtaining the necessary data, and as the field of Nuclear Physics was new, no adequate theories had been developed.

Within the past two decades, two valuable pieces of apparatus have been developed for the experimental study of Cosmic Rays. These instruments are the coincidence counter circuits employing Geiger-Muller (G.M.) counters and the counter controlled cloud chamber. With these instruments many valuable and accurate data have been obtained.

In 1936 the store of accurate experimental knowledge concerning Cosmic Rays was such that it was then possible to determine the charge of the particles, their energy spectrum, and their mass. A theory had also been developed to explain the experimental results. This theory was that the Cosmic particles were electrons with positive and negative charges and with an energy spectrum extending to energies of the order of 10^{12} e.v. Most of the experimental data which had been collected could be satisfactorily explained by this theory. The few

exceptions led to a revision of the accepted theory to one which would account for all of the observed experimental facts.

These outstanding exceptions were: (1) The breakdown of the theory for particles with energies greater than 2×10^8 e.v., (2) inconsistency between curvature, range, and ionization measurements in cloud chamber photographs of high energy Cosmic Ray tracks, and (3) the anomalous absorption coefficient for high energy Cosmic Ray particles.

(1) The theory then accepted satisfactorily explained the action of Cosmic particles with energies up to 2×10^8 e.v. assuming that they were electrons. Above this energy however the theory broke down. Particles with energies greater than 2×10^8 e.v. reacted differently--they did not all lose large amounts of energy by radiation as the theory predicted for electrons. This discovery led to the division of the Cosmic Ray spectrum into two parts, one with energies below 2×10^8 e.v. classed as the soft component, and the other with energies above 2×10^8 e.v. classed as the hard component.

Experimental results then seemed to indicate that the soft component is made up of electrons with energies extending up to 2×10^8 e.v. These electrons obey the Quantum Theory rules for energy loss as expressed by Heitler.[17,18] The hard component is made up of particles with energies greater than 2×10^8 e.v. These particles do not obey the

rules for energy loss by radiation as the particles in the soft component do. Now, since these particles could not be accounted for on the basis of Heitler's theory for electrons, it appeared as if the theory is valid only up to a certain limit of energy $E = 2 \times 10^8$ e.v., above which, it fails to work.

Now, according to Heitler's theory, which will be discussed in more detail later, an electron with energy greater than a certain critical value E_c will lose its energy by radiation. This critical energy depends on the absorber[17] -- $E_c = 1.3 \times 10^8$ e.v. for air and water, and 10^7 e.v. for Lead. Since most Cosmic Ray electrons have energies greater than 10^7 e.v., they should lose their energy by radiation when passing through any dense absorber.

An electron will lose nearly all of its energy in the form of a few hard light quanta in passing a short distance through an absorber. This distance[17] is 280 meters for air and 0.36 centimeters for Lead. The hard light quanta produced will travel in the same direction and will have energies comparable with the energy of the incident electron. These quanta generate electron pairs with energies also comparable with the original energy. The process is then repeated, each electron losing its energy in the form of more hard light quanta. This is the cascade process of shower production.[17] Since a certain amount of energy will

be lost at each transformation, eventually the energy will drop below the value E_c and be entirely dissipated.

Absorption experiments indicate that the most energetic electrons ($E \gg 2 \times 10^8$ e.v.) are highly absorbed by 10 cm. of Lead.[17,19,29] In contrast to this, the particles making up the hard component can penetrate more than 100 cm. of Lead, and some have been detected at a depth 800 m. below sea level.[41]

(2) The second exception was observed in cloud chamber photographs.[38] In these photographs several tracks were observed which showed a greater ionization than that of an electron track. This seemed to indicate a particle of greater mass than an electron. However, the range and curvature of the track showed that a proton could not have made it, since a proton having such a range would produce a track with a much greater radius of curvature.

(3) The third exception was observed in absorption measurements of the hard component.[32,27,5] It was observed that the apparent absorption coefficient was greater in air than in an equivalent amount of absorber in gms/cm.^{2} of a denser material such as Lead. Roughly speaking, The absorption coefficient varies inversely as the density of the absorber, but not inversely as the atomic number, since tests in air and carbon show very different absorption coefficients, although their atomic numbers are quite similar.[5]

These definite exceptions indicated that the theory then accepted was not giving the complete explanation. Heitler,[17] Bhabha,[6] Yukawa[44,45,46] and Euler and Heisenberg[12] have all contributed to the development of the new theory which satisfactorily explains the hard and soft component and the anomalous absorption of the hard component. The significant parts of the present theory will be presented briefly with the main emphasis on the research problem.

The energy loss for high energy electrons is explained satisfactorily by Heitler.[17] His theory holds for electrons even of the highest energies ($E >> 10^8$ e.v.) It will be outlined briefly in order to explain the reasons leading to the postulation and the discovery of the Mesotron, the heavy particle making up the hard component.

In Heitler's theory, the two methods by which an electron can lose energy are (a) radiation, and (b) collision.

(a) An electron passing through an electric field will be deflected. This deflection is equivalent to an acceleration of the electron so there is a radiation of energy in the form of light quanta. For high energy electrons the radiated energy is comparable to the energy E of the electron itself. The total mean energy loss/cm. path by radiation is[17]

$$-\frac{\partial E}{\partial x}\Big)_{rad} = NZ^2\left(\frac{e^2}{mc^2}\right)^2 \frac{E}{137}\left[21 - 4/3 \log Z\right] \qquad (1)$$

This energy is lost in the form of a few hard light quanta which are radiated in the same general direction as that in which the electron is traveling.

(b) An electron passing through the electronic shell of an atom suffers an inelastic collision and loses some of its energy. This collision energy loss/cm. path is

$$-\frac{\partial E}{\partial x}\Big)_{coll.} = 2\pi N Z \left(\frac{e^2}{mc^2}\right)^2 m_e c^2 \log \frac{E^3}{2mc^2 I^2 Z^2} \qquad (2)$$

where, as in equation (1) N equals the number of atoms/cm.^{3}, Z equals the atomic number and I equals the mean ionization energy (13.5 volts for air).

In comparing the two equations, we observe that the energy loss by radiation is proportional to Z^2,* while the collision loss is proportional to Z. If the main loss is by radiation, then there would be a much greater loss in dense materials. This does not agree with experimental results for the hard component. Also, since $\left(\frac{\partial E}{\partial x}\right)_{rad.}$ increases in proportion to E, there will be a certain critical energy E_c where the radiation loss equals the collision loss, and above this value the main loss will be by radiation. The values for this critical energy are 1.3×10^8 e.v. for air and 10^7 e.v. for Lead. Since most of the particles making up the hard component have energies greater than 10^8 e.v., they should suffer a large radiation loss in dense absorbers if they are electrons. This effect has not been observed in experiments.

*(except for the local factor which changes slowly with Z.)

A very extensive investigation of the specific energy loss of Cosmic Rays with energies up to 10^9 e.v. has been made by Neddermeyer and Anderson,[2] and Blackett and Wilson.[8,9] The experimental results showed that in the energy range up to 2×10^8 e.v., the specific energy loss for most of the particles is exactly as Heitler's theory predicts. In the energy range above 2×10^8 e.v., most of the particles do not obey the rules for specific energy loss. In both ranges, there appeared to be exceptions-- some particles with energy above 2×10^8 e.v. acted as electrons, while some with energies below 2×10^8 e.v. did not act as electrons. It appears as if the particles making up the entire energy spectrum are of two types-- one type containing particles with energies mainly below 2×10^8 e.v. which can be identified as electrons by Heitler's theory, and the other type containing particles mainly above 2×10^8 e.v. which cannot be accounted for by Heitler's theory. This leads to the conclusion that the hard component contains no electrons, and that there is no limit of energy above which Heitler's theory fails for electrons. In this classification, the hard and soft components do not occupy separate energy ranges; instead, the the distinguishing feature is that they are made up of different types of particles, and not of electrons of all energy ranges.

In equation (2) the energy loss through ionization by collision in a given material depends only on e, since in equation (2) the m_e outside of the logarithm is the mass of the extranuclear electrons in the atoms in the absorber and not the mass of the colliding particle. Hence the particle must have the same charge as an electron since the ionization loss is the same for particles in both the hard and soft components. Also, in equation (1) the energy loss by radiation depends on both e and m and is inversely proportional to m^2. Evidently the mass m of the hard component particle is greater than that of an electron since its loss by radiation is less. Now the energy loss by collision becomes a minimum for E greater than 2×10^8 e.v. This indicates that the mass of the particle cannot be greater than $\frac{2 \times 10^8}{C} = 400\, m_e$.

Experimentally, the mass of the particle in question can be determined from cloud chamber photographs of suitably chosen tracks which show greater than a minimum of ionization. Although such photographs(36,28,35) are not common, some tracks have been observed where E is less than 2×10^8 e.v. and the ionization is great enough for a determination of the mass of the particle. The resulting values for the mass vary between 160 and 400 electron masses(43) with a large probable error in each case.

Although the experimental evidence indicating the existence of the heavy particle was not definitely obtained until 1937[2] a theory postulating such a heavy particle was introduced by Yukawa in 1935.[44] His theory was introduced primarily to account for the internuclear forces existing at extremely short ranges (3×10^{-13} cm.) between the proton and neutron. Since the internuclear force cannot be electromagnetic, Yukawa introduced a new type of field which was assumed to satisfy a differential equation automatically leading to the observed short range forces (3×10^{-13} cm.). Instead of the electrostatic potential which satisfies the equation

$$\nabla^2 \varphi = 0 \qquad (3)$$

with a solution e/r, Yukawa's potential obeyed the differential equation

$$\nabla^2 \varphi + \lambda^2 \varphi = 0 \qquad (4)$$

with a solution

$$\varphi = g/r \, e^{-\lambda r} \qquad (5)$$

where g is a constant of the dimension of charge and $1/\lambda$ is the "Compton Wave Length" of the Mesotron (heavy particle). Now since the solution of equation (5) leads to forces with a range $1/\lambda$, Yukawa set $1/\lambda = 3 \times 10^{-13}$ cm. to account for the range actually observed.

Now this new field must be quantized. Instead of the light quanta arising from the electromagnetic field satisfying

a wave equation of the type

$$\nabla^2\varphi - 1/c^2 \frac{\partial^2\varphi}{\partial t^2} = 0, \qquad (6)$$

the wave equation for the Yukawa potential is of the type

$$\nabla^2\varphi + \lambda^2\varphi - 1/c^2 \frac{\partial^2\varphi}{\partial t^2} = 0. \qquad (7)$$

This is the DeBroglie wave equation for a particle with a rest mass

$$m = \frac{\lambda\hbar}{c} \doteq 150\, m_e.$$

Another difference between the nuclear field and the electric field is that the nuclear field leads to the exchange force between protons and neutrons. Yukawa explained this by assuming that the heavy particles corresponding to this exchange force are charged, so that a Mesotron can be virtually exchanged by a proton and neutron without any change occurring in the total charge. That is, a proton could emit a virtual Mesotron which would be absorbed by the neutron, the neutron becoming a proton and the proton becoming a neutron. The action is not permanent, since the proton does not become a neutron permanently. To completely account for the nature of this exchange force it is necessary also to assume that the Mesotron obeys Bose statistics and has a spin of 1.(12,7)

Yukawa(44,45) further assumed that an exchange action exists between the nuclear field and the light particles (electrons and neutrinos). For example, a very energetic electron can, due to the action of the field of force, emit

a negatively charged Mesotron and at the same time change into a neutrino. Similarly the Mesotron itself can (without any reciprocal action with other matter) decay into an electron and a neutrino. The Mesotron thus possesses a natural radioactivity.

The lifetime of the Mesotron is dependent on the strength of the exchange forces as is the lifetime of elements in β-activity. Consequently it is natural to assume that the two phenomena can be explained in the same way. Yukawa used the Fermi theory of β-decay and the strength of the exchange forces and calculated that the rest lifetime of the Mesotron is $\tau_0 = 5 \times 10^{-7}$ seconds.

Nordheim(29a) using the same assumptions and method calculated a value of $\tau_0 \doteq 10^{-8}$ seconds. His method is as follows: The probability of finding a Mesotron in the neighborhood of a proton-neutron pair in a nucleus is of the order of 1/10 (ratio of the binding energy per particle and the rest energy of the Mesotron). The lifetime τ_N of a nucleus subject to β-decay should therefore be 1/10 the lifetime τ_M of the Mesotron if just enough energy is available to create one. In Fermi's theory, $\tau_N \propto \epsilon_0^{-5}$ where ϵ_0 is the maximum energy of electrons emitted. Therefore

$$\tau_M / \tau_{N(\epsilon_0)} \propto \mu/M \left(\frac{\epsilon_0}{\mu}\right)^5 \qquad (8)$$

where μ and M are the rest energies of the Mesotron and proton. The lifetime of light elements of $\epsilon_0 \propto 5m$ is of the order of 100 seconds. If this is applied in equation (8) τ_M becomes of the order of 10^{-7} seconds.

Calculations of the lifetime from experimental data for Cosmic Ray Mesotrons indicate a value of τ_M of the order of 10^{-6} seconds. In order to get a comparable value of τ_M by using equation (8) it is necessary to decrease μ below the minimum value indicated by experimental results. An alternative is to increase τ_N. Now τ_N becomes greater for heavier radioactive elements so if we consider equation (8) to be correct, then we must assume that the Mesotron reaction can occur only in the heavy elements. This does not agree with experimental data which show that Mesotrons are produced in the atmosphere.

Apparently the Fermi theory of β-activity cannot adequately explain the problem of Mesotron disintegration, and the β-activity of radioactive elements cannot be considered as the same type of reaction as Mesotron disintegration.

If the theory of Mesotron disintegration is applied to the experimental data for the hard component in Cosmic Rays, the anomalous absorption effect referred to on page 4 can be explained.

The Mesotron can, with a certain lifetime, travel a distance depending on its velocity before disintegration. If Mesotrons of a definite velocity (momentum) pass through

a layer of air, more of them will disintegrate than if they pass through an equivalent amount of Lead in gms/cm.^{2} Since the disintegration would decrease the number of Mesotrons passing through the layer of air, the absorption ~~in air~~ would be due mainly to the disintegration, and it would be greater in air than in an equivalent amount of Lead in gms/cm.^{2} Further, since on disintegration the Mesotron would give off a high energy electron in the direction of its own motion, there will be an increase in the number of electrons present at sealevel in addition to those produced by cascade showers in the soft component. The effects have been observed experimentally by several workers. Euler and Heisenberg[12] have used this argument concerning the absorption and the disintegration electrons and applied it to the experimental results of Ehmert on the absorption of the soft and hard component. From it, they obtain a value of $\tau_o = 2.7 \times 10^{-6}$ secs.

Since it first appeared, Yukawa's theory has been modified by Yukawa,[45,46] Bhabha,[7] Heitler and Kemmer[21] to account for all of the experimental results obtained. The accepted theory now is that the hard component of Cosmic Rays is made up of Mesotrons of positive and negative charge, a mass of approximately $200m_e$, and a lifetime of the order of 1 to 3 microseconds. As yet, no definite values have been determined for the mass and lifetime of the Mesotron--nor is it certain whether such values are unique.

Now since the Mesotrons have a very short lifetime, they must be secondary particles produced by other particles at some height in the atmosphere. A Mesotron, in passing through the atmosphere, will lose a certain amount of energy depending on how far it travels. If the height for Mesotron production is assumed sufficiently great, then the Mesotron must become an electron before reaching the earth and it will be observed as an electron. If the height is assumed sufficiently small, then the Mesotron will reach the earth with a large amount of energy before it disintegrates. In order to make any definite evaluation of the lifetime from the intensity and energy at sealevel the height for production must be known. Also, since methods now used solve for the ratio of μ/τ_0, then the mass of the Mesotron must be known definitely in order to find τ_0.

If one wishes to make an accurate study of Mesotron intensity for different energies, all accompanying radiation must be eliminated. The usual method of elimination is to screen out the soft radiation by means of an absorbing screen. The usual screen consists of a Lead block 10 cm thick. The disadvantage of this method is that a Mesotron must have a certain minimum energy E_{min} in order to penetrate this absorber. All Mesotrons with less energy than this are eliminated, hence a complete energy spectrum cannot be obtained by this method.

The present research has been attempted primarily to

determine the true absorption curve for Mesotrons for absorber thickness starting at 1.5 cm. of Lead and extending up to 22.5 cm. in order to determine the energy spectrum for Mesotrons for this absorption region, and to determine the rest life-time of Mesotrons in this energy range.

ANALYSIS OF METHOD

After Yukawa postulated the existence of the Mesotron and indicated that it is an unstable particle with a very short lifetime, most of the investigators in the field of Cosmic Rays turned their attention to the problem of measuring the mass and lifetime of the Mesotron. Many different methods were used and many values resulted, as is indicated in TABLE I, shown on page 17. Here in TABLE I, a list of values of τ_o, the investigators, the methods and assumptions adopted, and the references are listed.

In TABLE I it appears that the value of τ_o depends on the method used, and the assumptions adopted regarding the height of production of Mesotrons, the energy distribution, and the mass of the Mesotrons.

In the method used in this research, several assumptions have also been made but an attempt is made to justify these assumptions. We choose $\mu = 10^8$ e.v. (200 m_e) as the mass of the Mesotron. Also, since the height of Mesotron production is not known definitely, the value of τ_o will be calculated assuming that Mesotrons originate at several different heights between 16 kilometers and 24 kilometers. Since it seems quite likely that τ_o is single-valued, the assumed height of production which gives the least deviation in τ_o for Mesotrons of different momenta will be chosen

TABLE I

Table of Measurements of τ_0 Made by Other Investigators

Value in μ seconds	Author	Method	Reference
1.7	Blackett	Absorption methods (vertical and inclined) at two different heights with $X_1 = 28$ KM and $m = 150\ m_e$	Nature. 142: 992. 1938.
1.6	Barnothy and Ferro	Absorption measurements (vertical and inclined) with wood above counter in vertical position	Phys. Rev. 60: 154. 1941.
1.2	Nielson and Ryerson	Absorption measurements (vertical and inclined) with graphite as absorber in vertical position	Phys. Rev. 59: 547. 1941.
2.4	Rossi and Hall	Momentum measurements	Phys. Rev. 59: 226. 1941
1.7	Clay	Differential momentum spectrum $E \propto E_0^{-2.93}$ $X_1 = 20$ KM	Rev. Mod. Phy. 11: 287. 1939.
4.1	Montgomery et. al.	Burst frequency	Rev. Mod. Phy. 11: 259. 1939.
3.1	Rasetti	Delay coincidence circuits	Phys. Rev. 59: 615. 1941

as correct.

If the Mesotron has a finite lifetime, it can travel a certain distance before disintegration, depending on its velocity (or momentum). Now, of the Mesotrons produced at a certain height, the number reaching sea level will depend on their original momenta. Hence it is important to know the momentum distribution at the place of origin. This can be determined by assuming a certain momentum at sea level and applying the equation of momentum loss for Mesotrons in reverse. In this way, it is possible to find how much momentum a Mesotron must start with at any height in order to reach sea level with a certain momentum. Or, if we know the Mesotron momentum spectrum at sea level we can determine the momentum spectrum at any assumed height of production of Mesotrons. Now we can determine the momentum spectrum at sea level from the Mesotron absorption curve and the Momentum-Range curve for Mesotrons for a Lead absorber. If we assume some relationship between the ratio of different numbers of Mesotrons at their origin, and ratio of their corresponding momenta, it is possible to calculate a value of τ_0 for these Mesotrons arriving at sea level with any momenta.

In the mathematical analysis of this method, the Rossi[30] system of units will be used. In this system, the velocity of light $c=1$, and the momentum $p=\frac{e.v.}{c}$ will be measured in electron volts. For the remaining terms the following symbols

will be used:

μ_e = rest energy of electron $= 5 \times 10^5$ e.v.,

μ = rest energy of Mesotron $= 10^8$ e.v. $= 200 m_e$,

χ_1 = the assumed height for production of Mesotrons,

$r_o = e^2/mc^2$ = classical radius of the electron,

Z = atomic number of the absorber,

I = ionization potential $= 13.5$ volts for air,

n = number of atoms/cm^3,

W_m = maximum energy transferable by a Mesotron on collision,

Subscript 1 indicates value at height χ_1,

Subscript 0 indicates value at sea level,

$\beta = v/c$

N_1 is the number of Mesotrons originating at χ_1 with momentum p_1,

N_0 is the number of N_1 Mesotrons remaining at sea level with momentum p_0,

$L(x)$ is the mean distance a Mesotron will travel before decay.

Now at height χ, the number of Mesotrons starting with momentum p is N where

$$\frac{dN}{N} = \frac{dx}{L(x)} \qquad (1)$$

From definition,

$$L(x) = T\beta = \frac{T_0 \beta}{\sqrt{1-\beta^2}} = \frac{T_0 p_x}{\mu} \qquad (2)$$

Combining equations (1) and (2) we have

$$\int_{N_0}^{N_1} \frac{dN}{N} = \frac{\mu}{T_0}\int_0^{x_1} \frac{dx}{p_x}, \quad \text{or} \quad \log \frac{N_1}{N_0} = \frac{\mu}{T_0}\int_0^{x_1} \frac{dx}{p_x}. \tag{3}$$

Now(31)

$$\frac{dp}{dx} = -\frac{2\pi n e^4 Z \mu_e}{m^2 c^4 \beta^3}\left[\log \frac{W_m \mu_e \beta^2}{I^2 Z^2 (1-\beta^2)} + 1 - \beta^2\right]. \tag{4}$$

Since it is desirable to have W_m in terms of momentum, W_m must be changed as follows: From principles of conservation of energy we have

$$W_m = \frac{\mu}{\sqrt{1-\beta^2}} - \frac{\mu}{\sqrt{1-\beta_1^2}} = \frac{m}{\sqrt{1-\beta_2^2}} - m, \tag{5a}$$

and from conservation of momentum we have

$$\frac{\mu\beta}{\sqrt{1-\beta^2}} - \frac{\mu\beta_1}{\sqrt{1-\beta_1^2}} = \frac{m\beta_2}{\sqrt{1-\beta_2^2}}; \tag{5b}$$

now

$$\frac{\mu}{\sqrt{1-\beta^2}} = (p^2+\mu^2)^{1/2},$$

so

$$p = \frac{\mu\beta}{\sqrt{1-\beta^2}} \qquad \text{and} \qquad \frac{\beta^2}{1-\beta^2} = \frac{1}{1-\beta^2} - 1.$$

Applying these relations in equations (5a) and (5b) we get

$$\frac{\mu}{\sqrt{1-\beta_1^2}} = \sqrt{p^2+\mu^2} - W_m \qquad \text{and} \qquad \frac{1}{\sqrt{1-\beta^2}} = \frac{W_m}{m} + 1,$$

also

$$\frac{\mu\beta_1}{\sqrt{1-\beta_1^2}} = \mu\sqrt{\frac{1}{1-\beta_1^2} - 1} = \mu\sqrt{\left(\frac{(p^2+\mu^2)^{1/2} - W_m}{\mu}\right)^2 - 1}$$

$$= \sqrt{\left((p^2+\mu^2)^{1/2} - W_m\right)^2 - \mu^2},$$

and

$$\frac{\beta_2}{\sqrt{1-\beta_2^2}} = \sqrt{\left(\frac{W_m}{m} + 1\right)^2 - 1}.$$

If we place these values in the momentum equation (5b), we get

$$p - \sqrt{(p^2+\mu^2)^{1/2} - W_m)^2 - \mu^2} = m\sqrt{\left(\frac{W_m}{m}+1\right)^2 - 1}$$

$$= \sqrt{W_m^2 + 2m W_m} \doteq W_m + m ,$$

since $W_m \gg m^2$.

If we transpose p and square both sides, we get

$$\left((p^2+\mu^2)^{1/2} - W_m\right)^2 - \mu^2 = \left(p - W_m - m\right)^2,$$

or

$$p^2+\mu^2+W_m^2 - 2W_m\sqrt{p^2+\mu^2} - \mu^2 = p^2 + W_m^2 + m^2 - 2pW_m - 2m(p - W_m)$$

Since m^2 is very small compared with μ, p, or W_m it can be neglected. The value of W_m in terms of μ and p then becomes:

$$W_m = \frac{mp}{\sqrt{p^2+\mu^2} - p + \mu}$$

The resulting value of W_m is now substituted in equation (4). The result is

$$-\frac{dp}{dx} = \frac{2\pi n e^4 Z \mu_e}{m^2 c^4 \beta^3}\left[\log \frac{\mu_e m p \beta^2}{I^2 Z^2 (1-\beta^2)\left(\sqrt{p^2+\mu^2} - p + \mu\right)} + 1 - \beta^2\right]. \quad (7)$$

Eliminating β by the expression $\beta = \left(\frac{p^2}{p^2+\mu^2}\right)^{1/2}$, we get

$$\frac{dp}{dx} = -\frac{2\pi n e^4 Z \mu_e}{m^2 c^4}\left(\frac{p^2+\mu^2}{p^2}\right)^{3/2}\left[\log \frac{\mu_e m p^3}{I^2 Z^2 \mu^2 \left(\sqrt{p^2+\mu^2} - p + m\right)} + \frac{\mu^2}{p^2+\mu^2}\right] \quad (8)$$

Eliminating m gives

$$\frac{dp}{dx} = -n 2\pi r_0^2 Z \mu_e \left(\frac{p^2+\mu^2}{p^2}\right)^{3/2}\left[\log \frac{\mu_e p^3}{200 I^2 Z^2 \mu \left(\sqrt{p^2+\mu^2} - p\right)} + \frac{\mu^2}{p^2+\mu^2}\right] \quad (8a)$$

By rearranging equation (8) we get

$$n\,dx = \frac{1}{2\pi r_0^2 Z \mu_e}\left(\frac{p^2}{p^2+\mu^2}\right)^{3/2}\frac{dp}{\log\frac{\mu_e p^3}{200 I^2 Z^2 \mu(\sqrt{p^2+\mu^2}-p)}+\frac{\mu^2}{p^2+\mu^2}} . \qquad (9)$$

Now $n = n_0 e^{-\alpha x}$, where x = height in centimeters. So we have

$$\int_0^{x_1} e^{-\alpha x}dx = \frac{1}{2\pi n_0 r_0^2 Z \mu_0}\int_{p_0}^{p_1}\frac{\left(\frac{p^2}{p^2+\mu^2}\right)^{3/2}dp}{\log\frac{\mu_e p^3}{200 I^2 Z^2 \mu(\sqrt{p^2+\mu^2}-p)}+\frac{\mu^2}{p^2+\mu^2}} \qquad (10)$$

Let us call the integrand of the right hand side P and

$$\int_{p_0}^{p_x} P\,dp = \Sigma .$$

Then we have

$$\Sigma = \int_0^{x_1} e^{-\alpha x}dx = -\frac{1}{\alpha}\left(e^{-\alpha x_1}-1\right), \qquad (10a)$$

from which we get $$x = -\frac{1}{\alpha}\log\left(1-\alpha\Sigma\right) . \qquad 10b$$

Now if Σ is evaluated for any value of p_x then we can solve for a corresponding value of x. Equation (3) contains $\int_0^{x_1}\frac{dx}{p_x}$, so if the reciprocal of the values of p_x are calculated and plotted against x and the resulting curve integrated, the integral in equation (3) is obtained for any value of x. We now have

$$\log\frac{N_1}{N_0} = \frac{\mu}{T_0}a , \qquad (12)$$

where

$$a = f(p_0, x) = \int_0^{x_1}\frac{dx}{p_x} . \qquad (12a)$$

Now let us consider two groups of Mesotrons γ and δ of numbers $N_{1\gamma}$ and $N_{1\delta}$ at x_1 and $N_{0\gamma}$ and $N_{0\delta}$ at sea level ($x = 0$). Here γ and δ are subscripts differentiating between two groups of Mesotrons, and 0 and 1

have their usual assigned meaning. $N_{o\gamma}$ and $N_{o\delta}$ are the numbers of Mesotrons absorbed by a unit thickness of absorber at any two chosen values of absorber thickness. Applying equation (12) we have

$$\log \frac{N_{1\delta}}{N_{o\delta}} - \log \frac{N_{1\gamma}}{N_{o\gamma}} = \mu/T_o \left(a_\delta - a_\gamma\right) \qquad a_\delta = \int_o^{x_1} \frac{dx}{p_{i\delta}(x)}$$

then

$$\mu/T_o = \frac{1}{a_\delta - a_\gamma}\left[\log \frac{N_{1\delta}}{N_{1\gamma}} \cdot \frac{N_{o\gamma}}{N_{o\delta}}\right] = \frac{1}{a_\delta - a_\gamma}\left[\log \frac{N_{o\gamma}}{N_{o\delta}} + \log \frac{N_{1\delta}}{N_{1\gamma}}\right]$$

Now let us assume as Heisenberg[16,32] does that

$$\frac{N_{1\delta}}{N_{1\gamma}} = \left(\frac{p_{1\delta}}{p_{1\gamma}}\right)^c \qquad \text{where } c \doteq -2.9$$

Then we have

$$\frac{\mu}{T_o} = \frac{1}{a_\delta - a_\gamma}\left[\log \frac{N_{o\gamma}}{N_{o\delta}} + c \log \frac{p_{1\delta}}{p_{1\gamma}}\right] \qquad (13)$$

The values of a_δ and a_γ are determined as explained previously for two different values of p_x at a definite height x_1. The values of $N_{o\gamma}$ and $N_{o\delta}$ can be obtained from an absorption curve for Mesotrons. $p_{1\gamma}$ and $p_{1\delta}$ can be determined from the range of Mesotrons of momenta $p_{o\gamma}$ and $p_{o\delta}$ at sea level corresponding to $p_{1\gamma}$ and $p_{1\delta}$ at a height x_1.

The main value of this mathematical treatment lies in the results which can be obtained by its use. In order to show the value of this method the actual results obtained will now be given. The values of a_γ and a_δ are obtained from Graph 7, the values of $p_{1\gamma}$ and $p_{1\delta}$ are obtained from Graph 9, and the values of $N_{o\gamma}$ and $N_{o\delta}$ are obtained from the experimental absorption curve for Mesotrons given

in Graph 2. This graph represents the final results of the experimental work done in this research.

In this method, three assumptions are made: μ is chosen as $200m_e$, C is chosen as -2.9, and χ_1 is chosen at several different values. The sensitivity of the value of τ_o to these assumptions can be observed on inspection of the values of τ_o obtained. The computations giving the values of a_γ and a_δ, and $\rho_{1\gamma}$ and $\rho_{1\delta}$ are given further on in this paper. TABLE II gives values for N, ρ, and a for values of $\chi_1 = 16$, 20, 21, 22, 22.5, 23, and 24 KM. The values of τ_o are calculated for the different heights and momenta and are tabulated in TABLE III.

In the numerical calculation of τ_o, the right hand side of equation (13) must be multiplied by $\frac{e}{300c}$ to convert to the correct units. In equation (13) $\frac{1}{a_\delta - a_\gamma}$ is momentum and is measured in electron volts. On the left hand side, $\mu = 200m_e = 200 \times 9 \times 10^{-28} = 18 \times 10^{-26}$ gms.

$$\text{Now } \frac{e}{300c} = \frac{4.8 \times 10^{-10}}{9 \times 10^{12}} = 0.53 \times 10^{-22}.$$

If we substitute these values in equation (13), we get a value of

$$\tau_o = \frac{18 \times 10^{-26}}{0.53 \times 10^{-22} \times R.H.S.} = \frac{3400 \times 10^{-6}}{R.H.S.} \text{ seconds.}$$

Values of ρ, N, and a are now taken from TABLE II and applied in this equation. The equation is then solved for τ_o, the rest lifetime of the Mesotron.

TABLE II

Values of N, A and P for Different Ranges R in Lead and Assumed Heights X_1

Range in Lead in cm.	N	X_1=16 KM		X_1=20 KM		X_1=21 KM	
		$p \times 10^{-8}$	$a \times 10^{5}$	$p \times 10^{-8}$	$a \times 10^{5}$	$p \times 10^{-8}$	$a \times 10^{5}$
0	.08	21.4	187.5	22.29	205	22.7	209.8
1	.09	21.55	178	22.41	199	22.8	203.
2	0.105	21.7	168.5	22.58	192	23	195.
3	0.12	21.86	160	22.75	184	23.16	187.
4	0.14	22.1	151	22.91	178	23.3	180.5
6	0.17	22.34	145	23.26	166	23.6	170.
8	0.19	22.64	139	23.6	158.2	23.94	161.
10	0.21	22.95	133	23.95	151.7	24.24	155.
15	0.30	24.36	117	25.47	132.	25.66	137.

(continued)

TABLE II

(Continued)

A	N	X_1 = 22 KM		X_1 = 22.5 KM		X_1 = 23 KM		X_1 = 24 KM	
		pX 10^{-8} e.v.	aX 10^{5}	pX 10^{-8}	aX 10^{5}	$pX10^{-8}$	$aX10^{5}$	$pX10^{-8}$	$aX10^{5}$
0	.08	22.94	213.2	23	216.2	23.1	218.6	23.3	222.9
1	.09	23.09	205.5	23.15	209	23.24	211.8	23.44	216
2	.105	23.23	197.5	23.31	200.4	23.4	204	23.61	208
3	.12	23.4	189	23.46	193	23.54	197	23.76	200
4	.14	23.55	183	23.61	186	23.71	189	23.92	193
6	.17	23.86	172.4	23.94	175	24.09	176.5	24.24	181.5
8	.19	24.18	165	24.25	167	24.34	170	24.55	173.2
10	.21	24.5	159.4	24.56	161	24.66	163.5	24.86	167
15	.30			26.00	142	26.10	144.2	26.30	148.

TABLE III

Values of τ_0 in Micro-Seconds for Different Assumed Heights for Mesotron Production ($C = -2.9$)

Thickness in cm. of Lead	X_1 16 KM τ_0	X_1 20 KM τ_0	X_1 21 KM τ_0	X_1 22 KM τ_0	X_1 22.5 KM τ_0	X_1 23 KM τ_0	X_1 24 KM τ_0
0 and 1	2.22	1.37	1.67	1.79	1.73	1.59	1.60
" 2	2.04	1.4	1.60	1.68	1.70	1.56	1.60
" 3	1.98	1.52	1.68	1.79	1.72	1.6	1.67
" 4	1.88	1.44	1.56	1.62	1.62	1.58	1.60
" 6	1.64	1.52	1.56	1.58	1.62	1.64	1.62
" 8	1.59	1.50	1.64	1.64	1.63	1.69	1.65
" 10	1.58	1.53	1.62	1.58	1.62	1.64	1.65
" 15	1.40	1.44	1.47		1.50	1.51	1.53

at $R_1 = 0$ cm and $R_1 = 10$ cm $\quad X_1 = 24$ Km

$$R.H.S. = \frac{10^5}{223 - 167}\left(\log \frac{.08}{.21} - 2.9 \log \frac{24.86}{23.3}\right) = 2065$$

$$\tau_0 = \frac{3400 \times 10^{-6}}{2065} = 1.65 \mu \text{ seconds}$$

$C = -2.5$

Thickness in cm of Lead	X_1 20 KM τ_0	X_1 22.5KM τ_0	X_1 24 KM τ_0
0 and 1	1.40	1.72	1.68
" 2	1.47	1.78	1.65
" 3	1.53	1.73	1.70
" 4	1.45	1.64	1.62
" 6	1.53	1.64	1.65
" 8	1.60	1.67	1.70
" 10	1.57	1.65	1.68

$C = -3.5$

X_1 20 KM τ_0	X_1 22.5 KM τ_0	X_1 20 KM τ_0
1.31	1.67	1.63
1.39	1.70	1.61
1.49	1.68	1.68
1.41	1.60	1.59
1.49	1.60	1.69
1.55	1.63	1.65
1.52	1.60	1.63

The values of τ_o are listed in TABLE III. The results show that the values of τ_o are dependent on χ, and C. Now if we can assume that the values of χ, and C which will give the least variation in τ_o for Mesotrons of different momenta are correct, then the height of Mesotron production is $\chi = 24$km., $C = -2.9$, and $\tau_o = 1.63 \pm 0.04 \times 10^{-6}$ seconds.

The value of τ_o is also dependent on the slope of the Mesotron intensity curve at different thicknesses of Lead absorber. The curve can be changed to give a wide variation in τ_o and still be within the limits of probable error in the experimental results. Since it is believed that τ_o has a definite value which does not change, then it seems logical that the correctly drawn curve should show the least resulting variation. Several different curves were drawn through the experimental points on the Mesotron intensity curve in order to find the one which gives the smallest variation in τ. The most satisfactory curve is shown in Graph 2. It is interesting to note that it lies well within the limits of probable error.

As mentioned before, this method is not a simple clear method of evaluating τ_o, and its accuracy is necessarily not great, since a certain amount of error will enter into the evaluation of the integral for momentum loss and there is some experimental error in the graph of atoms/cm.^{3} as a function of height. Its main value lies in the fact that

it gives a very good indication as to the height for production of Mesotrons, and it gives a value of τ_0 for Mesotrons over the low energy end of the Mesotron energy spectrum. Most investigators assume a definite height for Mesotron production and base the accuracy of their value of τ_0 on the assumption that the chosen height is correct. The method discussed in this work gives consistent values of τ_0 for Mesotrons with ranges up to 10 cm. of Lead, but for the higher energy Mesotrons the calculated value of τ_0 decreases appreciably. If we assume that the absorption curve is more accurate above a range of 10 cm. of Lead, then we would have to increase the slope of the curve below 10 cm. in order to get a correspondingly small value of τ_0 over this range. Since other rather accurate methods indicate a higher value of τ_0 ;[11,33] the more logical explanation of the apparent decrease in the value of τ_0 for high energy Mesotrons is that the very penetrating Mesotrons are produced at a lower altitude than the low energy Mesotrons, and the absorption curve is drawn correctly over the range from 0 to 10 cm of Lead. It seems more likely that Mesotrons of different energies are produced at different heights, rather than that they have different values of τ_0 or μ. This theory of variation in height for Mesotron production will be discussed further in the Appendix with reference to recent work done by Hall[16] and Regener.[30]

DESCRIPTION OF EXPERIMENTAL APPARATUS

The apparatus used in this research consisted of a coincidence counter circuit capable of recording both triple and quadruple coincidences. The counters used were of the conventional style and size used by most workers in the field of Cosmic Rays. Since part of the research was in building and testing these counters, this work will be described in detail.

These G.M. counters had an overall length of 11 inches and were 1¼ inches in diameter. The cylindrical electrodes were made of thin copper tubing 8 inches long and 1 inch in diameter. The center wires were of 3 mil tungsten.

A special treatment was given these counters in order to obtain a stable counter with a wide voltage plateau. The treatment used is as follows: The copper cylinder and tungsten center wire were first sealed inside a Pyrex glass envelope with the cylinder electrode at one end and the center wire electrode at the other end. The actual electrodes were of 10 mil tungsten sealed in the two ends of the glass envelope. The 10 mil tungsten wire was spot welded to the copper cylinder and the 3 mil center wire. One end of the center wire was embedded in the glass so that only one electrode was available for external connection. This made it impossible to flash the wire by an application of a low

potential across the center wire. The flashing of the wire which was to outgass the wire and remove any sharp points was accomplished by another method which will be described later.

After assembly, the insides of the counters were washed thoroughly with concentrated HNO_3, then rinsed with 3N. HNO_3, 1N. HNO_3, and 0.1N. HNO_3. After this they were rinsed with distilled water, and a final rinsing of Ethyl Alcohol. They were then dried by blowing dry compressed air into them. This treatment left the copper cylinders with a shiny pale violet coloring.

The next step in the treatment was to connect the counters to the vacuum system so that they could be outgassed and evacuated. The counters were sealed to a glass frame inside of a cylindrical electric furnace. Below this furnace was a high vacuum pumping system. This vacuum system consisted of a Mercury diffusion pump which fed the air it pumped out of the vacuum chamber into a Cenco Hi-vac pump. This pumping system by itself was capable of pressures as low as 10^{-5}mm. Lower pressure was obtained by means of a liquid air trap. The outgassing process was carried out as follows: The Cenco Hi-vac pump was started and the pressure in the counters reduced. The counters were carefully tested for leaks by means of a high voltage spark coil. All seals and glass connections were tested. When no leaks were found,

this same high voltage spark coil was connected to the two electrodes of one of the counters. A strong glow discharge first appeared but after a period of 10 minutes the glow had disappeared. The pressure was kept constant at about 10^{-2} mm. during this process. The same procedure was carried out for each of the counters in turn, until no discharge was visible. It was noticed that if the Cenco pump was not kept running during this process, the pressure rose slightly,so the pump was kept running. This operation is not critical, so it isn't necessary to keep the pressure too constant.

The next step was the pumping and baking process. The electric furnace was turned on and kept constant at a temperature of 400°C. This temperature was kept constant by means of a thermocouple and galvanometer arrangement which indicated the temperature at all times. The diffusion pump was turned on at the same time, and the counters were pumped and baked for four hours. At the end of this time, the furnace was turned off and removed. At this stage the counter walls were covered with a thin copper film caused by evaporation of some of the copper during the baking and pumping process. This film was removed by heating the counter walls with a small gas flame.

The counters were now ready to be oxidized. The vacuum system was turned off and dry air was admitted into the system at atmospheric pressure. The counters were again heated with

the gas flame until a thin red oxide coating appeared on the copper cylinders.

The counters were now ready to be filled with gas to the proper pressure. Several different gases such as argon, hydrogen, air, alcohol vapor and mixtures of these gases have been used by different workers.[22,39,40] Air was chosen for these counters. The pumping system was again turned on and the pressure reduced to 10^{-4} mm. Dry air was again admitted to a pressure of about 7cm. This operating pressure was determined by counting and voltage plateau tests. A counter circuit was connected to each counter in turn and the pressure was varied until the voltage plateau was widest at a reasonable operating voltage(1500 volts). Figure A shows a view of the complete G.M. counter and a graph showing the voltage plateau characteristics of one of these counters.

Sixteen counters were manufactured by this process, and by varying the pressure in each tube before it was sealed off, it was possible to make all of them operate at the same voltage. During this testing it was found that too low pressure caused spurious counting, gave no appreciable plateau, and gave a very low operating voltage. Too high pressure caused the operating voltage to be very high and there was only a very narrow plateau.

Each counter was sealed off when its pressure had been adjusted correctly. After its removal, all of its seals and

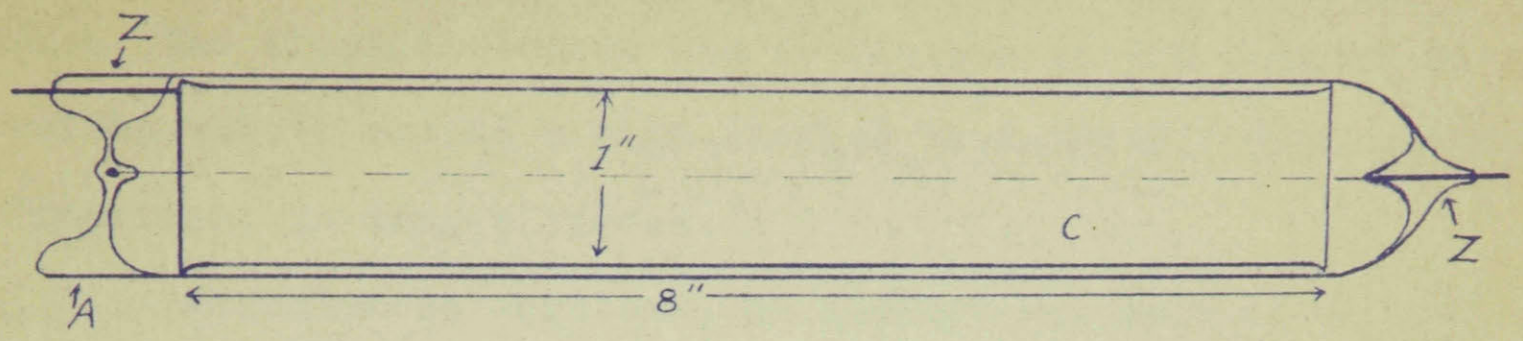

A – Air Seal

Z – Tungsten Seal

C – Copper Plate

Geiger-Müller Counter

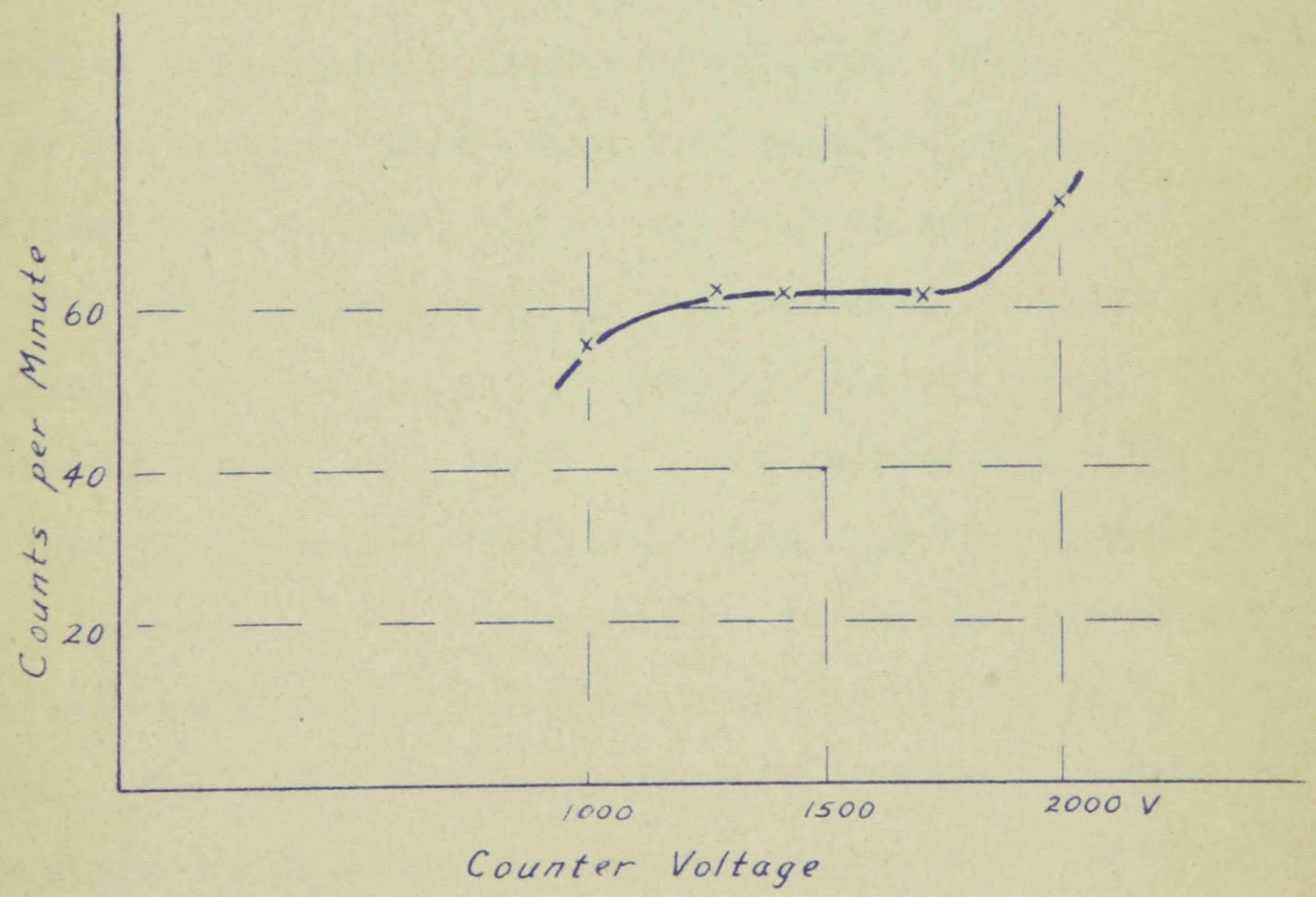

Voltage Plateau Curve

Fig. A

electrodes were covered with pycine wax to prevent future leaks. The final treatment was to dip the entire counter in hot paraffin wax to create a high surface resistance. This waxing is important in damp climates.

In making these counters, no attempt was made to follow methods outlined previously by other workers in the field. The different steps were taken first to make sure the copper was perfectly clean, completely outgassed during treatment, and finally given a low potential threshold. The pressure was chosen because it gave the widest voltage plateau at a reasonable operating voltage. Actually, the voltage plateau was much wider than required, since a stabilized high voltage supply was used on the counters.

The circuit diagram for the coincidence circuit used is shown in Figure 1. In the drawing, all resistors, capacitors, tubes, etc. which are not labeled are identical with the corresponding ones above them. In the analysis of the operation of this circuit all resistors, tubes and capacitors referred to are those given in the circuit diagram. The complete counter circuit is able to detect both triple and quadruple coincidences and record them on separate mechanical recorders.

The triple coincidence circuit consists of three resistance coupled amplifiers with one common load resistance. The quadruple coincidence circuit is another

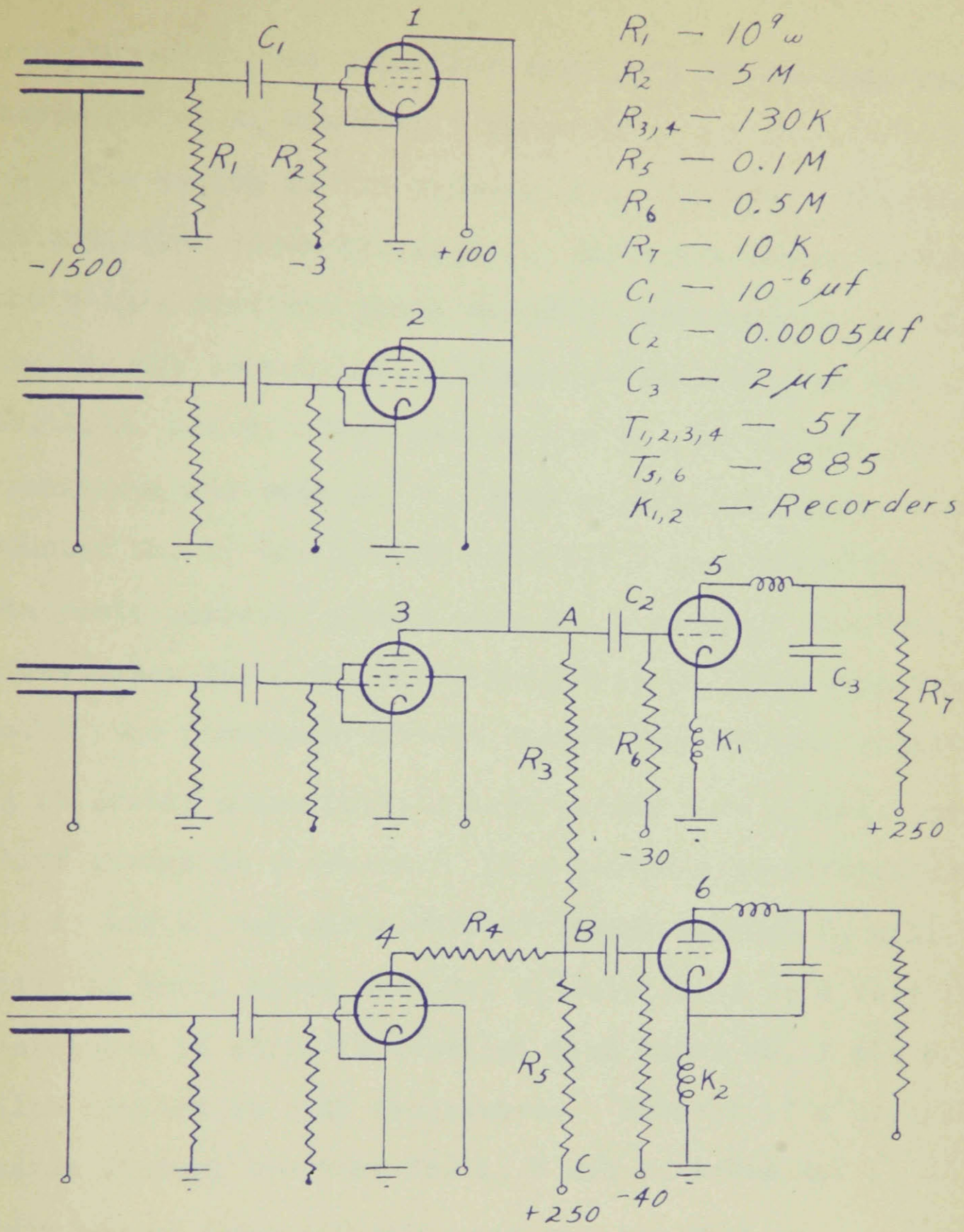

Coincidence Counter Circuit

Fig. 1

resistance coupled amplifier with part of its load resistance common to the triple circuit.

The action of the circuit is as follows. The grids of amplifier tubes No. 1, 2, 3, and 4 are biased so that there is a constant plate current. Resistors R_3 and R_5 make up the common load resistance for amplifier tubes No. 1, 2, and 3. Resistors R_4 and R_5 make up the load resistance for tube No. 4. When a particle passes through counter No. 1, the grid of tube No. 1 goes negative and the plate current through tube No. 1 ceases. However, since tubes No. 2 and 3 are hooked in parallel with tube No. 1, the resultant current change through load resistor R_3 is small, hence point A experiences only a small positive change in potential. If a particle penetrates counters No. 1, and 2, the plate current change through R_3 will still be small since tube No. 3, which acts as a very low resistance is still in parallel with tubes No. 1 and 2 which now act as high resistances. However if a particle passes through counters No. 1, 2 and 3, tubes No. 1, 2 and 3 become non-conducting and point A will become much more positive due to the large decrease in the IR drop across R_3. Point A is coupled by means of C_2 to the grid of the thyratron tube No. 5. When point A becomes positive enough to make tube No. 5 flash, a large current flows through counter K_1 which records a triple count.

As condenser C_3 discharges, the plate voltage on the thyratron drops to zero and the tube again becomes non-conducting. At the same time point A becomes positive, point B will also become positive, but not as much as point A since some current is still flowing through counter amplifier No. 4. If the grid of tube No. 6 is biased more negatively than tube No. 5 it will not fire under the above current change. However, if a particle passes through all four counters, the plate current drops to a very low value, points A and B become positive enough to cause both thyratrons to fire and triple and quadruple counts are recorded. A particle passing through any single counter will not cause either of the thyratrons to flash. Only when counters No. 1, 2 and 3 or all four counters are hit will one or both of the thyratrons flash.

Any number of counters can be hooked together in this parallel arrangement for detecting coincidences. The size of pulse required to cause the thyratrons to fire depends on the grid bias on the thyratron and the size of the coupling condenser C_2.

The quenching circuit used on the counters consisted of a high resistance R_1 of 10^9 ohms placed between the center wire of the G.M. counter and ground. A negative potential of 1500 volts was put on the cylinders of the G.M. counters. The counter was coupled to the grid of its

amplifier through a condenser C_1 of $10^{-6}\mu$ fds. made by waxing a brass cylinder around R_1 and using R_1 as one condenser plate. The time constant of such a circuit is $= R_1 C_1$ which equals 10^{-3} seconds.

The recovery time of the circuit depends on how far above the counting voltage threshold the counters are operated. If the operating voltage is too high, the recovery time will be long, since it will take more time for the potential of the wire to drop below the threshold voltage. For best results counters which operate at the same voltage should be used, then the operating voltage can be quite close to the threshold voltage. The recovery of the complete circuit was found to be 9×10^{-4} seconds. This value was determined by use of Auger's[4] formula for the determination of accidentals if the recovery time is known. The four G.M. counters were removed from the lead shield and placed in a horizontal plane. The number of accidentals occurring was counted over a period of time and applied in the equation

$$N = \frac{n^x t^{x-1}}{(60)^{x-2}}$$

where N = number of accidentals per hour

n = counting rate of a single counter per minute.

x = number of counters

t = resolving time in seconds.

This resolving time is admittedly not as fast as some

circuits[39,27,25,26] give, but since the triple counting rate was not too high (<60 counts per hour) the probability that a ray would penetrate counters No. 1, 2 and 3 during the inactive time of the circuit is very small. The probability is $W = 9 \times 10^{-4} \times \frac{1}{60} = 1.5 \times 10^{-5}$, a value which is too small to make any noticeable difference to the final experimental results.

One feature of this circuit is that each of the counters must be shielded electrostatically. This feature was used to some advantage by making the shields big and sturdy enough that they could contain the amplifier tube and quenching circuit and also protect the counter from possible damage.

The counter shields were of aluminum tubing 18 inches long and $1\frac{3}{4}$ inches in diameter. The G.M. counter was placed in one end of the shield with the high voltage lead connected to an insulated terminal fastened in the end of the shield. The amplifier tube was mounted on a standard radio socket in the opposite end of the shield. A six contact socket was mounted at the end of the shield and all necessary voltage connections were made through this socket. The quenching circuit was connected between the counter and the grid terminal of the 57 amplifier tube.

The amplifier power supply was mounted on a chassis along with the thyratron circuits and mechanical recorders.

All connections between the amplifiers, voltage supply, and thyratron circuits were made by means of a six conductor cable leading from the chassis to the socket in each counter shield. The triple coincidence counter connections were made farthest from the chassis connections and the quadruple coincidence counter was mounted nearest to the chassis. There are seven conductors leading to the chassis, five of these for the common grid bias, heater supply, screen supply and cathode, the sixth for the triple coincidence plate supply, and the seventh for the quadruple coincidence plate supply.

The arrangement is very convenient since the connecting cable can be made quite long, thus allowing the counters to be placed some distance from the power supply. Also, if it is desired to measure the efficiency of any of the counters, any one of them can be disconnected from the circuit by pulling out the six-prong plug in the particular counter shield. This changes the circuit from a triple and quadruple coincidence circuit to a double and triple circuit. The efficiency of that particular counter which has been disconnected will be the ratio of the counting rate when all of the counters are in to the counting rate when that particular counter is removed, if the sensitive solid angle of the counter arrangement has not been changed, and correction is made for accidentals which are small in this case.

The power supply for the amplifier is shown in Figure 2. It is a conventional full wave condenser input power supply unit capable of supplying a maximum voltage of 300 volts at 100 ma.

The high voltage supply for the counters is a half wave rectified pentode stabilized circuit. The step-up transformer is a 3000 volt neon sign transformer supplying 3000 volts at 20 ma. The rectifier tube is a half wave mercury vapor type 866 tube. The rectified voltage is stabilized by a combination 22½ volt bias battery and a type 57 pentode. The voltage is filtered by means of an RC filter consisting of a 2 μfd. 3000 volt oil filled condenser and two one megohm resistors in series. Transformer T_1 is the high voltage transformer, and T_2 and T_3 are the filament transformers for the rectifier and the pentode. In these transformers the secondary windings are insulated for 3000 volts from the primary and the core. All fixed resistors in the circuit are I.R.C. wire wound precision resistors accurate to 1%. A complete analysis of this circuit is given in a paper by R. Evans.(13)

Two identical coincidence circuits were used in the research. One high voltage supply supplied the high potential for both circuits, since all of the counters operated over the same voltage plateau.

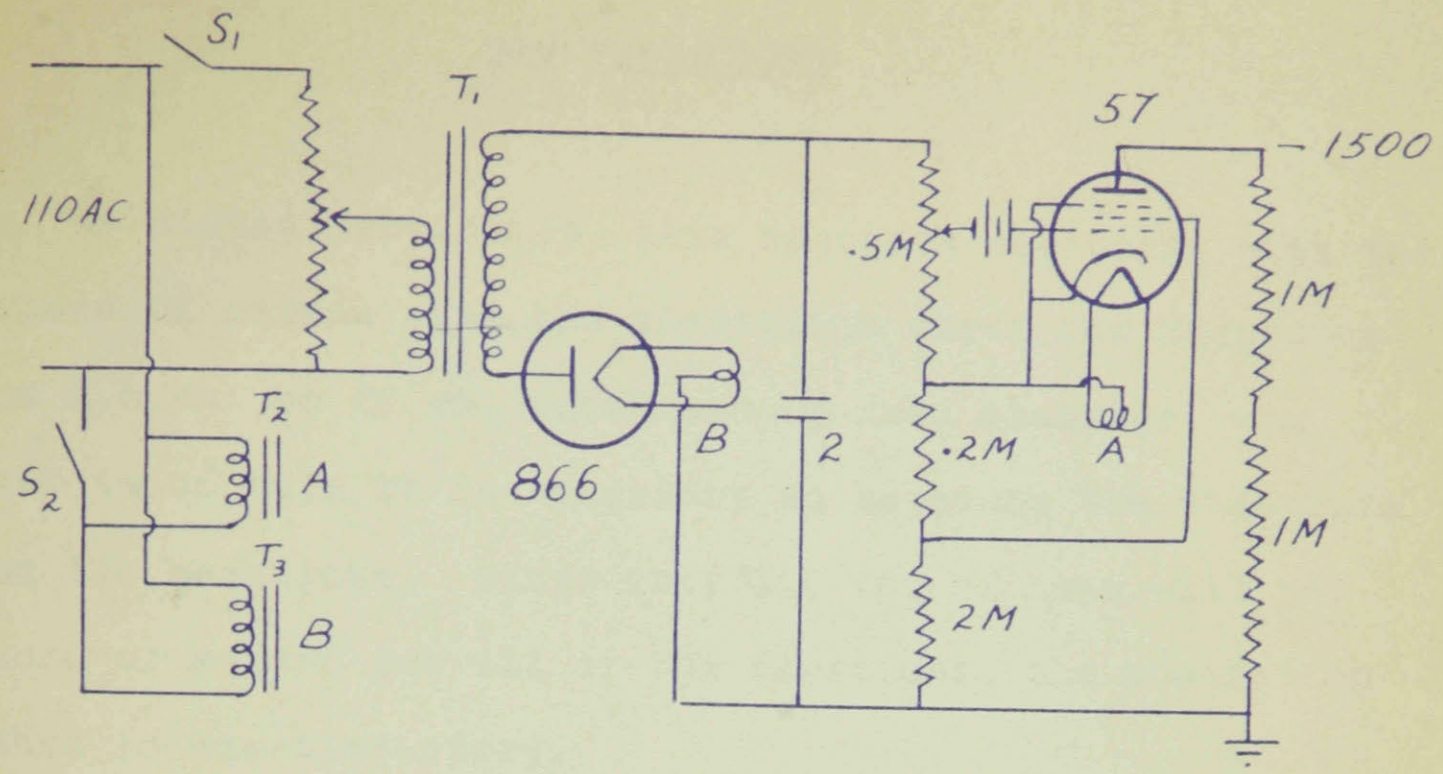

High Voltage Supply

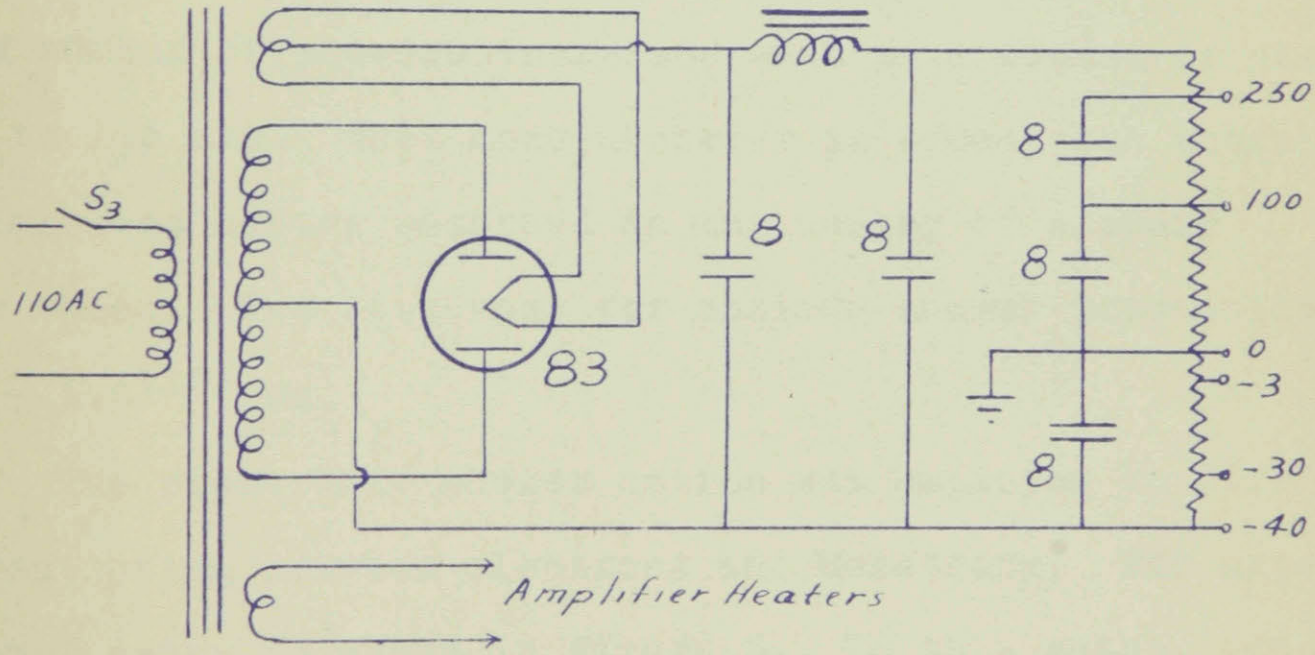

Amplifier Voltage Supply

Fig. 2

THE EXPERIMENT

As stated previously, this research was begun with the purpose of determining the absorption curve for Mesotrons from 1.5 cm. to 20 cm. thickness of lead absorber. In order to do this it is necessary to separate the electrons from the Mesotrons. Since only 1.5 cm. of Lead will not absorb or screen out all of the electrons, the absorption method is unsatisfactory.

The method of separation adopted was based on a characteristic action of electrons. It is well known that electrons, when passing through an absorber, create showers. The number of showers increases with an increase of absorber up to 1.5 cms. When more absorber is added, the showers themselves become absorbed so the number of showers decreases. The thickness for maximum shower production is $\doteq 1.6$[15] cm.

The electronic shower action was employed in differentiating between electrons and Mesotrons. The experimental setup is shown in Figure 5. In this setup, counters No. 1, 2 and 3 are placed in line while counter No. 4, which consists of two counters hooked in parallel, is placed so that it will not be hit by a particle going through counters No. 1, 2 and 3. The lead block A is the shower producer for electrons. The lead shield C is

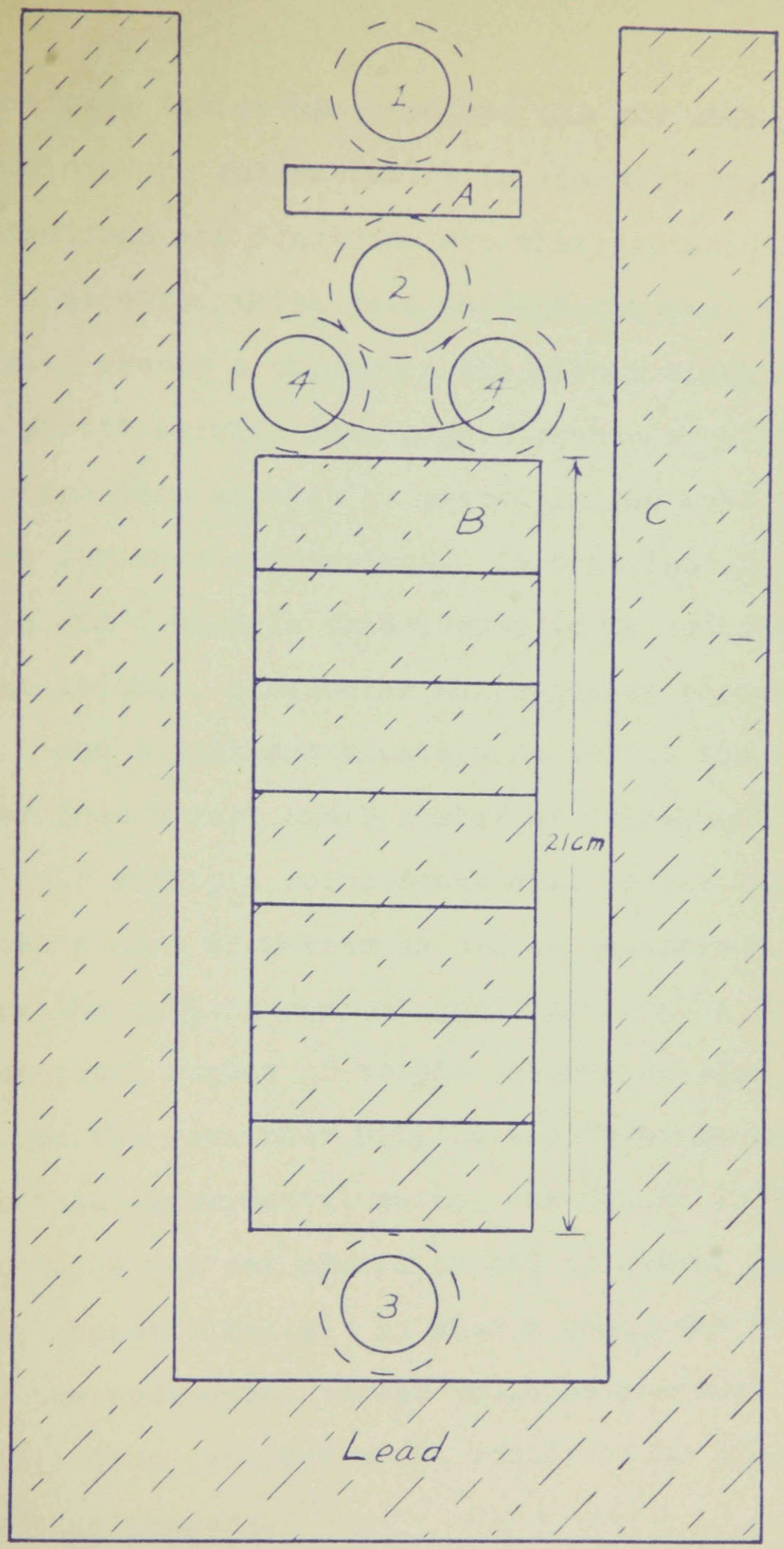

Counter Arrangement for
Separation of Electrons and Mesotrons

Fig. 3

placed around the setup to screen out any soft radiations from radioactive contamination in the vicinity.

Mesotrons and electrons are distinguished in this way. An electron which goes through counters No. 1, 2, and 3 will create a shower in the shower block A. These shower particles will have a good chance of hitting counter No. 4, since this counter is placed in the most favorable position for shower detection. This action will cause both a triple and quadruple coincidence to be recorded. In contrast to this, a Mesotron which passes through counters No. 1, 2 and 3 will not create a shower in the shower block A (other than a very small number of "knock-on" electrons). Hence, only a triple coincidence will be recorded. Now the total number of Mesotrons can be determined by subtracting the total number of quadruple counts (electrons) from the total number of triple (Mesotrons plus electrons) counts and the remainder will be the Mesotron count.

In this experimental setup, one defect is that counter No. 4 may not always be hit by shower particles from the shower block A. In such a case, the electron causing the undetected shower would be recorded as a Mesotron. Thus, counter No. 4 would not be 100% efficient in detecting showers.

The efficiency of counter No. 4 for shower detection was determined by means of the experimental setup shown

in Figure 4. In this arrangement, counter No. 1 is out of line with counters No. 2 and 3. Counter No. 4 is still in its usual position below the shower block A. A thin Lead plate D (5 mm. thick) is placed above counter No. 1. Now shower particles originating in Lead plate D which strike counters No. 1, 2 and 3 will pass through the Lead block A. Since the shower particles are definitely electrons, a shower should be started in the shower block A. If counter No. 4 is 100% efficient, every shower originating in block A will cause a quadruple and a triple count. If counter No. 4 does not detect these showers then only a triple count will be recorded. The efficiency of counter No. 4 will then be the ratio of quadruple counts to triple counts.

This efficiency test was carried out with absorber B varying from 0 to 9 cm. of Lead. The purpose of testing over this entire range was to see if the efficiency varied for incident electrons of different momentum. Since the size of the showers produced varies for electrons of different incident momenta the angle covered by counter No. 4 may not have completely covered the angle of the shower particles. The test was carried out for a period of 250 hours at each different absorber thickness. The final results obtained are not extremely accurate since the probable error is still quite high. However it does

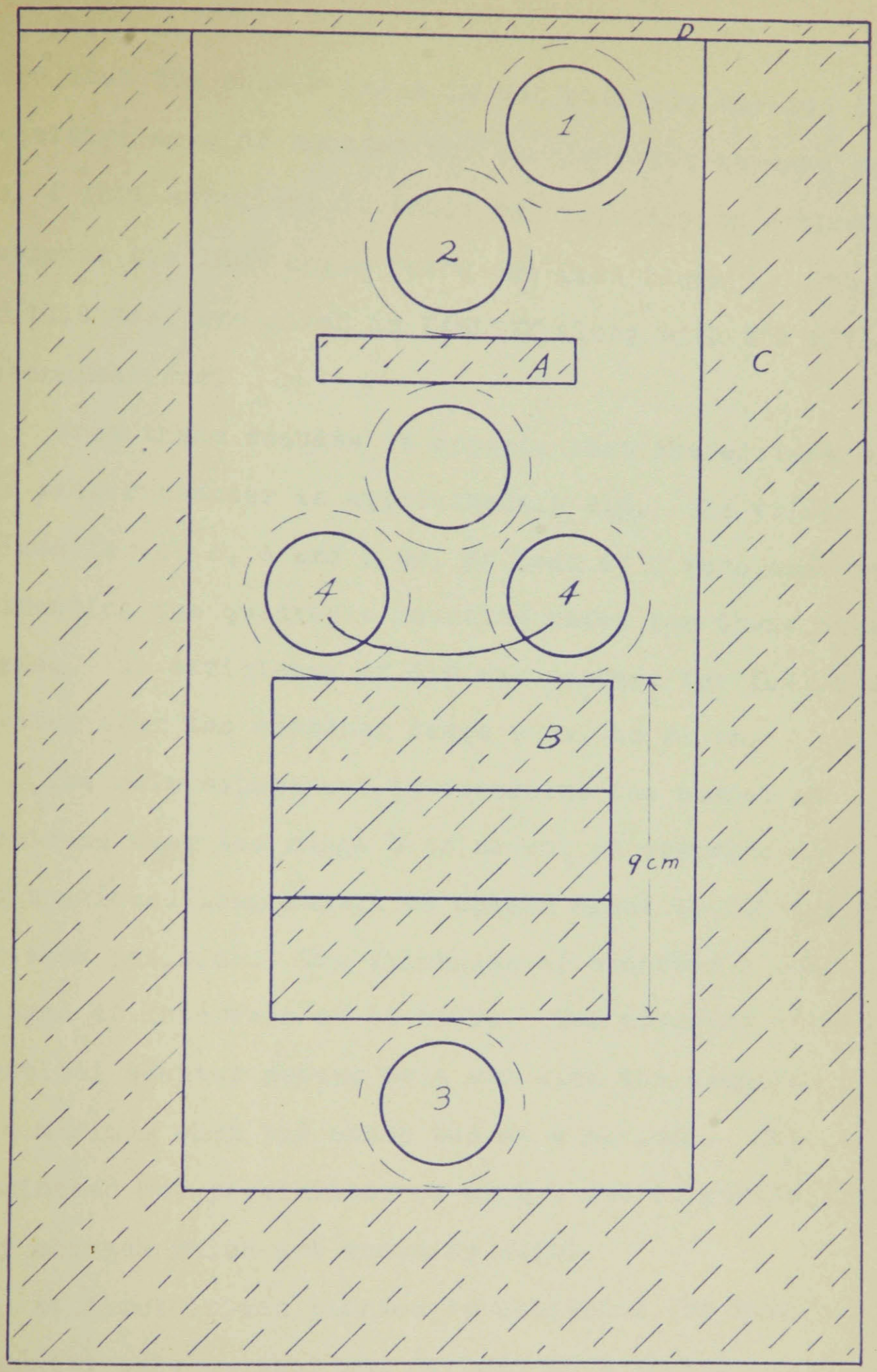

Arrangement for Measuring
the Effiency of Shower Counters

Fig. 4

show that the shower angle is not entirely covered by the sensitive area of counter No. 4. In order to make counter No. 4 100% efficient it would be necessary to entirely surround the 180° angle below the Lead block A. The results of this test are given in TABLE *IV* along with the efficiency determinations.

From these results it appears that the efficiency of the shower counter is approximately 61%. The values obtained for 0, 3, 6 and 9 cm. of Lead at B were used in correcting the quadruple counting rates for these thicknesses. An efficiency of 61% was assumed for the shower counter over the absorber range 9 cm. to 21 cm.

The main experiment to determine the number of Mesotrons over the range 0 to 21 cm. of absorber at B was continued long enough to obtain about 40,000 counts. for each position. The thickness of absorber B was changed at intervals of 50 hours. Two circuits with identical counter setups were run with the absorber in one at a maximum when the other was at a minimum. This action eliminated any possibility of errors due to general intensity changes which are known to exist.

At first it was planned to determine the Mesotron intensity only up to 9 cm. of Lead at B so the counters were set up allowing only 9 cm. of space between counters No. 3 and 4. Later when it was decided to take measurements

TABLE IV

Experimental Results Used in Determining

The Efficiency of The Shower Counter

Lead Thickness in cm. at B	Triples	Quadruples	Time *in hrs.*	Ratio (Efficiency)
0	1517	950	245	.626 ± .04
1½	1066	617	246	.578 ± .04
3	743	422	254	.570 ± .03
4½	543	285	248.5	.530 ± .05
6	518	318	268.5	.615 ± .05
7½	338	209	250	.620 ± .06
9	340	215	250	.630 ± .06

up to a maximum of 21 cm. at B, counter No. 3 had to be lowered. This decreased the solid angle covered by the counters, so the counting rate decreased.

At the conclusion of the experiment, all of the counting rates for the second setup ($B_{max.} = 21$ cm.) were multiplied by a constant factor to make them coincide with the higher counting rates of the first setup. The values for the triple and quadruple counting rates over the entire absorber range for the second setup have been adjusted in this manner. This set of values is given in TABLE V.

The tables of experimental values obtained are plotted on Graph 1 and Graph 2. Graph 1 is drawn from the quadruple counting rate as a function of the absorber thickness. Curve A is drawn through the experimental points obtained. Curve B is drawn through points representing the experimental results after corrections have been made for shower efficiency. From this curve we notice that the counting rate decreases from a fairly large value at 1.5 cm. of Lead to a low value at 10.5 cm. of Lead, then the counting rate remains approximately constant up to 22.5 cm. of Lead. This result is explained in this manner: The quadruple counting rate is not entirely due to shower particles caused by incident electrons, but partly due to "knock-on" electrons caused by Mesotrons passing through the shower block. Now other workers have shown that all electrons in Cosmic Rays

are absorbed by 10 cm. of Lead. If this is true, then the constant shower counting rate observed between 10.5 and 22.5 cm. of Lead is caused entirely by "knock-on" electrons and not by showers produced by electrons. In order to get the correct electron counting rate, this constant counting rate observed between 10.5 and 22.5 cm. of Lead must be subtracted from all shower counting rates between 1.5 and 22.5 cm. of Lead. The curve C drawn through these resulting points represents the true incident electron counting rate over the range of absorber investigated. This curve agrees quite well with theoretical curves depicting the energy spectrum of electrons.

Graph 2 represents the triple counting rate as a function of Lead absorber varying in thickness from 0 to 22.5 cm. of Lead. This thickness of absorber includes the 1.5 cm. Lead block used as a shower producer. In order to compare these results with those of some other investigator, values obtained by Clay[11] were plotted on the same curve. The agreement is quite good. The dotted curve represents the difference between the triple counting rate and the true electron counting rate as obtained in Graph 1.

The dotted curve represents the main object in the research. It is the Mesotron absorption curve for Mesotrons with ranges between 1.5 cm. and 22.5 cm. of Lead. As yet, no other experimental data for this region have been found published.

This experiment was performed in the attic store room of the Macdonald Physics Laboratory, McGill University, Montreal. The roof above the apparatus was a wooden one covered by thin copper sheeting. The counters were lined up with their axes at right angles to the magnetic meridian. This experiment was carried out over a period of time extending from January 1940 to September 1941.

TABLE V

Table of Experimental Results Giving

The Triple, Quadruple, and Electron Counting Rates

Thickness in cm. at B	Triples	Rate	Quadruples	Rate	Corrected Rate	Time in Hours
0	43110	62.1±0.2	7700	11.12±0.085	17.7	693
3	50820	53.5±0.16	4760	5.1 ±0.049	8.8	950.75
6	38415	50.0±0.17	2955	3.84±0.047	6.25	769
9	57570	49.2±0.14	3760	3.21±0.035	5.20	1170.75
12	48760	48.7±0.15	3645	3.64±0.04	5.8	1003
15	43640	48.4±0.16	3210	3.56±0.04	5.65	901.75
18	41095	45.6±0.15	2850	3.17±0.04	5.2	902
21	41045	44.9±0.15	2950	3.22±0.04	5.23	916

Graph 1

Experimental Results

Counts/Hour Plotted Against Lead Absorber

A × Original Shower Rate

B ⊙ Corrected Shower Rate

C △ Incident Electron Counting Rate

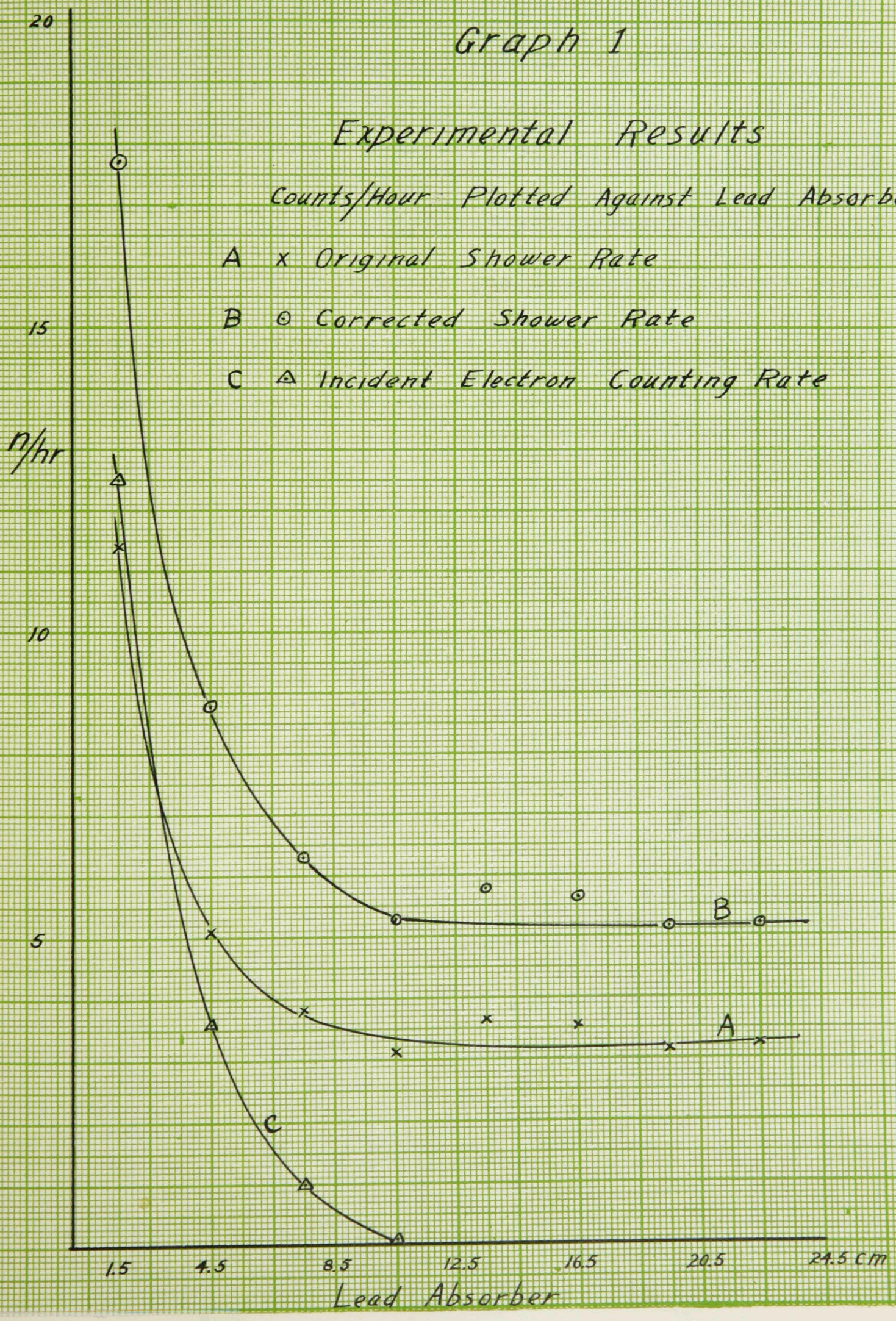

Graph 2

Experimental Results

Counts/Hour Plotted Against Lead Absorber

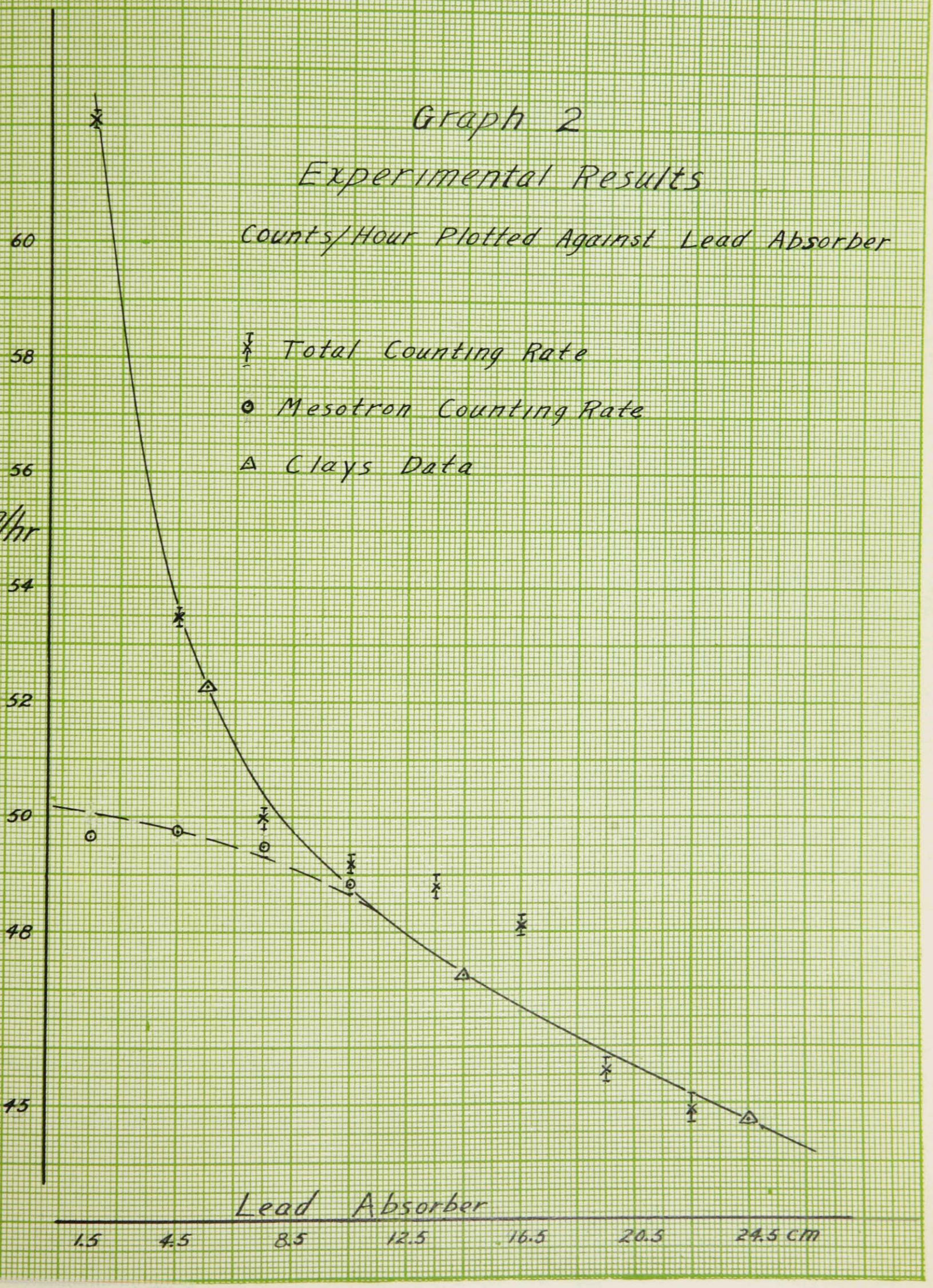

COMPUTATIONS LEADING TO THE VALUE OF THE MESOTRON LIFETIME

The mathematical treatment of the method used for measuring τ_0 follows. The numerical constants used in the treatment are listed below for convenience;

$\mu = 10^8$ e.v. = rest energy of the Mesotron,

$m = 9 \times 10^{-28}$ gms. $= 0.5 \times 10^6$ e.v. (μ_e),

$e = 4.8 \times 10^{-10}$ e.s.u.,

$C = 3 \times 10^{10}$ cm/sec. $= 1$ in Rossi units,

$N_0 = 2.705 \times 10^{19}$ molecules/cm.^{3}, $= n/2$ for Oxygen

$Z =$ atomic number of absorber

$= 14$ for Nitrogen,

$= 16$ for Oxygen,

$= 82$ for Lead,

$I =$ Ionization potential (15.5 volts for air),

$p =$ momentum in e.v.

Referring to the theoretical analysis, we see that the first problem is the integration of equation (10) which is

$$\int_0^x e^{-\alpha x} dx = \int_{p_0}^{p_x} \frac{m^2 c^4}{2\pi n Z \mu_e} \left(\frac{p^2}{p^2+\mu^2}\right)^{3/2} \frac{dp}{\log\left(\frac{\mu_e p^3}{200 I^2 Z^2 \mu \left(\sqrt{p^2+\mu^2} - p\right)}\right) + \frac{\mu^2}{p^2+\mu^2}}$$

The right hand side of this equation cannot be integrated by the usual integration methods. The method used is to plot the value of the integrand for values of p_x

from 0 to 25×10^{8} e.v. The left hand side of equation (10) is not exact since the value of α is not constant. However, since the actual experimental data are available which accurately describe the left hand side for values of

up to 28 kilometers, it is better to plot these values and equate areas under the resulting curve to corresponding areas under the curve of the right hand expression. By following this procedure it is possible to find a value of p for every value of x , i.e. if a Mesotron has a momentum of $p = 0$ at $x = 0$, then for any height x a corresponding value of momentum p can be calculated.

The right hand integrand is evaluated for values of momentum from $p = 0$ to 25×10^{8} e.v. using both Oxygen and Nitrogen as the absorbers. A weighted mean is taken (on the basis of 4 parts of Nitrogen to one part of Oxygen) of the two values for each momentum. This weighted mean then gives a value of the integrand for air.

In evaluating the right hand integrand p is varied continually over the entire momentum range. Since there are two constant terms not involving p , they are evaluated separately. They are:

$$\Gamma = \frac{m^2 c^4}{2\pi e^4 n Z \mu_e} \begin{cases} = 0.91 \times 10^{-2} & \text{for Oxygen} \\ = 1.04 \times 10^{-2} & \text{for Nitrogen} \end{cases}$$

and

$$\lambda = \frac{\mu_e}{200 I^2 Z^2 \mu} \begin{cases} = 2.14 \times 10^{-9} & \text{for Oxygen} \\ = 2.8 \times 10^{-9} & \text{for Nitrogen} \end{cases}$$

The integrand now can be written

$$\Gamma\left(\frac{p^2}{p^2+\mu^2}\right)^{3/2}\frac{1}{\log\frac{\lambda p^3}{\sqrt{p^2+\mu^2}-p}+\frac{\mu^2}{p^2+\mu^2}}=P$$

The values of P for $p=0$ to 25×10^8 e.v. for air are given in TABLE VI.

The values of P_{air} are plotted against p_x in Graph 3.

The experimental values satisfying the left hand side of equation (9) are tabulated in TABLE VII and plotted in Graph 4. The area under the curve is calculated by applying Simpson's Rule to the experimental points. The experimental data were obtained from two sources: Dynamische Meteorologie by Exner[14] and Physics of The Air by Humpherys.[20] Exner's data are given in terms of pressure and temperature. The values of N/N_o are determined from these data. Exner's data extend only to $\chi = 20$ kilometers. Humpherys' data for pressure extend to $\chi = 40$ kilometers but only to $\chi = 20$ kilometers for temperature. Since the temperature appears to be constant from 18 to 20 kilometers it was assumed constant up to 28 kilometers. Values of N/N_o for range $\chi = 20$ to $\chi = 28$ kilometers were calculated on this assumption. The values of N/N_o for the range $\chi = 20$ to 28 kilometers were also calculated by assuming that the values for $\chi = 14$ to 20 kilometers satisfy an exponential function $f(x) = e^{-\alpha\chi}$. This function was extended up to 28 kilometers. The difference between

TABLE VI

Evaluation of The Integrand $\Gamma\left(\frac{p^2}{p^2+\mu^2}\right)^{3/2} \frac{1}{\text{Log}\frac{\lambda p^3}{\sqrt{p^2+\mu^2}-p} + \frac{\mu^2}{p^2+\mu^2}}$ for Air for Values of p_x

p_x	$\left(\frac{p^2}{p^2+\mu^2}\right)^{3/2}$	$\frac{\mu^2}{p^2+\mu^2}$	$\text{Log}\frac{\lambda p^3}{\sqrt{p^2+\mu^2}-p}$ O_2	N_2	P_{O_2}	P_{N_2}	P_{air}
0	0	1			0	0	0
0.1 x10^8e.v.	.00098	0.991	10.05	10.31	0.81x10^{-6}	0.905x10^{-6}	0.886x10^{-6}
0.2 "	.0075	0.977	11.5	12.5	5.47"	5.77 "	5.7 "
0.4 "	.0512	0.864	14.58	14.75	3.1 x10^{-5}	3.42 x10^{-5}	3.36 x10^{-5}
0.5 "	.0895	0.800	15.20	15.50	5.08"	5.72 "	5.60 "
0.6 "	0.136	0.736	15.90	16.20	7.45"	8.39 "	8.22 "
0.8 "	0.244	0.620	16.90	17.20	12.7 "	14.17 "	13.8 "
1 "	0.352	0.500	17.75	18.0	17.6 "	19.8 "	19.4 "
1.5 "	0.576	0.308	19.4	19.6	26.5 "	30.2 "	29.5 "
2 "	0.716	0.200	20.4	20.6	31.6 "	35.7 "	34.9 "
3 "	0.854	0.100	22.0	22.2	35.0 "	39.7 "	38.8 "
4 "	0.915	0.0598	23.1	23.4	36.0 "	40.5 "	39.3 "
5 "	0.944	0.0392	24.1	24.4	37.0 "	40.0 "	39.5 "
6 "	0.960	0.0283	24.8	25.2	35.5 "	39.5 "	38.7 "
7 "	0.970	0.020	25.2	25.6	34.9 "	39.2 "	38.4 "
8 "	0.977	0.0156	25.9	26.2	34.3 "	38.6 "	37.8 "
10 "	0.986	0.0099	26.8	27.1	33.5 "	37.7 "	36.9 "
12 "	0.990	0.00702	27.5	27.8	32.6 "	37.0 "	36.1 "
16 "	0.995	0.00396	28.7	28.9	31.5 "	35.7 "	34.9 "
25 "							33.5 "

Graph 3

Integrand of Equation (10) Plotted Against p_x

× Air

⊙ Lead

P_a

P_l

p_x

4×10^{-4}

3

2

1

8×10^{-7}

7

6

5

4

3

2

1

0 1 2 3 4 5 6 7 8 9 10 11×10^8 ev.

TABLE VII

Relationship between Height χ and Number N of Atoms Per Cubic Centimeter and The Evaluation of The Integral $\int_0^{\chi} e^{-\alpha\chi} d\chi$ for Values of χ

χ in Km	N/N_0	$\int_0^{\chi} e^{-\alpha\chi} d\chi$
0	1	0
1	0.9	95,150
2	0.808	181,000
3	0.726	257,000
4	0.654	325,000
5	0.587	387,000
6	0.521	442,000
7	0.475	492,000
8	0.423	536,500
9	0.376	577,000
10	0.333	612,500
11	0.290	643,500
12	0.252	640,500
13	0.217	693,500
14	0.187	713,500

(Continued)

TABLE VII

(Continued)

x in Km	N/N_0	$\int e^{-\alpha x} dx$
15	0.158	730,500
16	0.134	745,000
17	0.115	757,500
18	0.096	768,000
19	0.0816	777,000
20	0.077	785,000
21	0.058	792,000
22	0.052	797,500
23	0.044	802,000
24	0.038	806,000
25	0.030	809,000
26	0.026	812,000
27	0.020	814,000
28	0.015	816,000

Graph 4

Experimental Results

N/N_0 of Atoms/cm^3 Plotted Against Height x

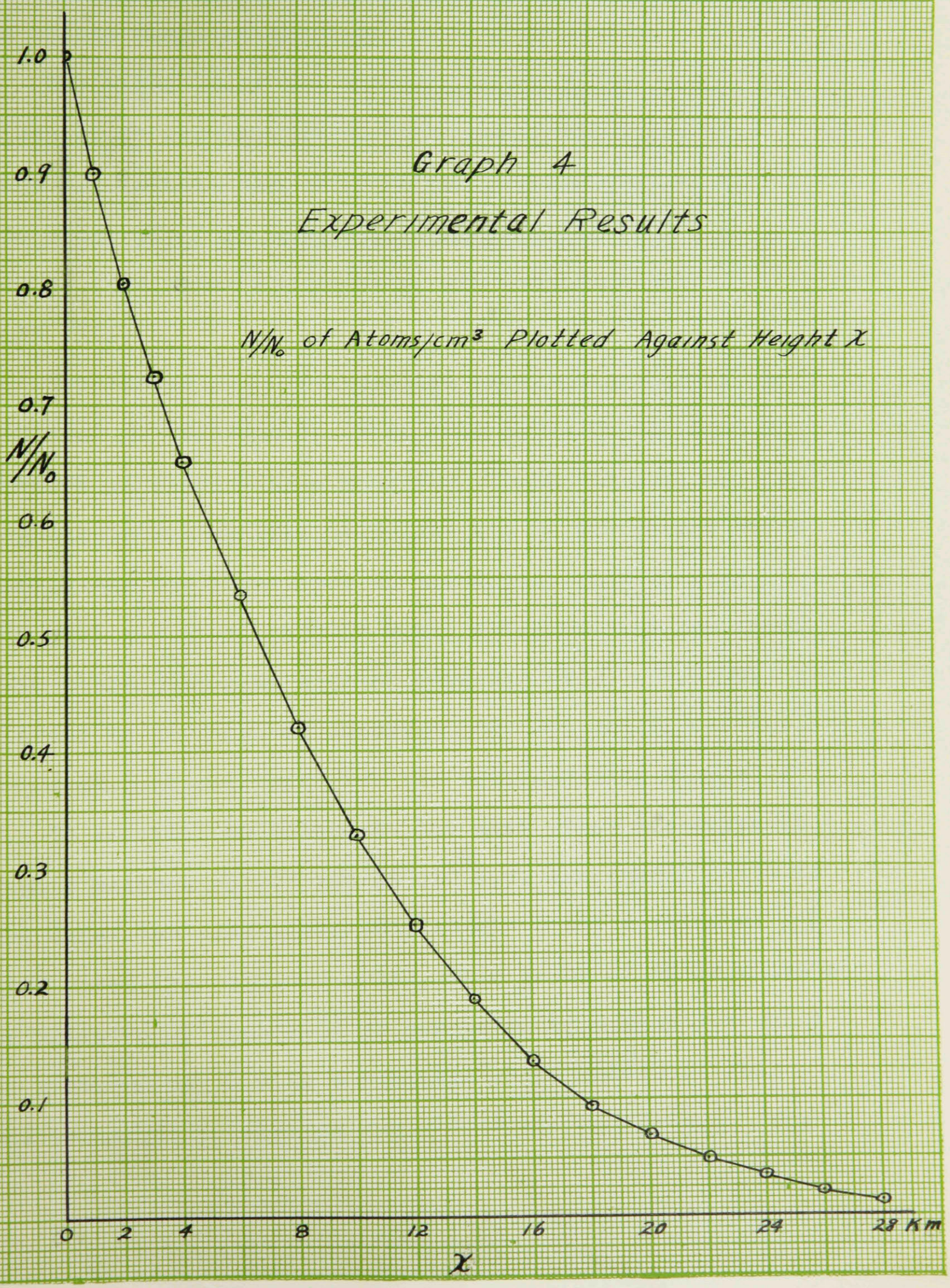

the two sets of values obtained is too small to make any observable change in the evaluation of the function over the entire range of altitude.

The areas under the curve in Graph 3 for different values of p_x are equated to areas under the curve in Graph 4. In this way, a value of χ corresponding to each value of p_x is obtained. These values of p_x, χ, and the area under the curve Σ are tabulated in TABLE VIII.

The values of p_x are plotted against corresponding values of χ in Graph 5. From this curve we see that a Mesotron produced with a momentum $p_1 = 23 \times 10^8$ e.v. at height $\chi_1 = 22.5$ KM will have lost all of its energy after penetrating the atmosphere to sea level. Now we wish to find what energy a Mesotron would still have at sea level if it started at some greater momentum at $\chi_1 = 22.5$ KM. In order to do this, we choose $p_1 = 24$, 25, and 26×10^8 e.v. at $\chi_1 = 22.5$ KM and solve for the corresponding values of p_o. To do this, we calculate the area under the curve in Graph 3 between $p_x = 23$ and 24×10^8 e.v. and equate it to an area under the same curve between $p_x = 0$ and a value of p_x which gives the required area. This value of p_x represents the momentum p_o possessed at sea level by a Mesotron which was produced at χ_1 with a momentum $p_1 = 24 \times 10^8$ e.v. This same technique is applied for $p_1 = 25$ and 26×10^8 e.v. The

TABLE VIII

Values of Momentum p_x as a Function of Height x and Evaluation of $\int_0^{p_x} P\,dp$ for The Values of p_x

$p_x \times 10^{-8}$	x in km	$\int_0^{p_x} P\,dp = \Sigma$
1	0.0707	7,050
2	0.376	35,600
3	0.756	72,900
4	1.192	112,000
5	1.70	151,500
6	2.12	191,000
7	2.48	229,500
8	3.16	268,000
10	4.47	343,000
11	4.80	380,000
12	5.50	416,000
14	6.90	487,000
15	7.68	522,000
18	10.4	627,000
20	13.1	696,000
22	17.8	765,000
23	22.5	799,500
24		834,000
25		868,000
26		902,000

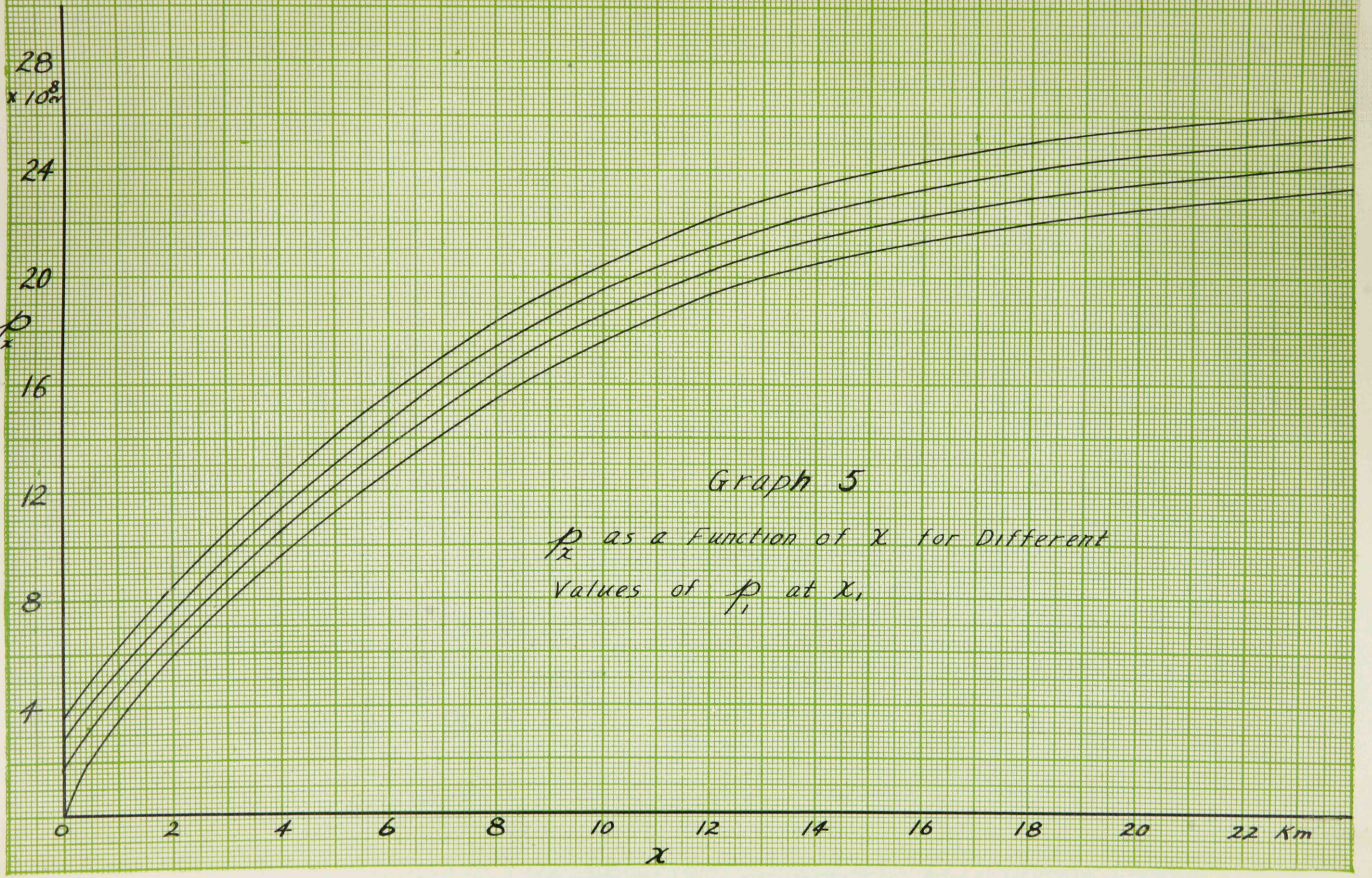

Graph 5

p_x as a Function of x for Different Values of p_1 at x_1

TABLE IX

Computations Used to Find p_0 for Different Values of p_1 at $x_1 = 22.5$ KM

$p_1 \times 10^{-8}$	$\sum$	$p_0 \times 10^{-8}$	$\Delta \sum$
23	799,500	0	0
24	834,000	1.96	34,200
25	869,000	2.9	69,200
26	902,000	3.7	102.300

resulting values of x, p_x, $\sum$, p_0 and $\Delta \sum$ are given in TABLE IX.

On Graph 5, p_x is plotted against x for $p_0 = 0$, 1.96, 2.9, and 3.7×10^8 e.v. It can be observed on this graph that the momentum difference between the four curves remains constant at unity for $x_1 = 16$ KM, 20 KM and 24 KM. The values of p_x and for $x_{p_0} = 1.96 \times 10^8$, $x_{p_0} = 2.9 \times 10^8$ and $x_{p_0} = 3.7 \times 10^8$ e.v. are given in TABLE X. Here we see that although Mesotrons may start out with unit momentum difference, they do not arrive at sea level with this unit difference.

The values of $1/p_x$ are now plotted against x for the four values of p_0. These curves are on Graph 6. The values are given in TABLE XI.

TABLE X

Relationship between Momentum p_z and

Height χ for Different Values of Momentum p_o

$p_z \times 10^{-8}$	χ in Km $p_o = 1.96 \times 10^8$ e.v.	χ in Km $p_o = 2.9 \times 10^8$ e.v.	χ in Km $p_o = 3.7 \times 10^8$ e.v.
4	0.81	0.42	--
6	1.72	1.28	0.92
8	2.73	2.21	1.82
10	3.75	3.22	2.7
12	4.92	4.35	3.83
14	6.2	5.6	4.9
16	7.7	6.9	6.4
18	9.4	8.5	7.74
20	11.65	10.45	9.55
22	15.1	13.15	11.72
24	22.5	17.7	15.04

Graph 6

$1/p_x$ Plotted Against x

(Reciprocal of Graph 5)

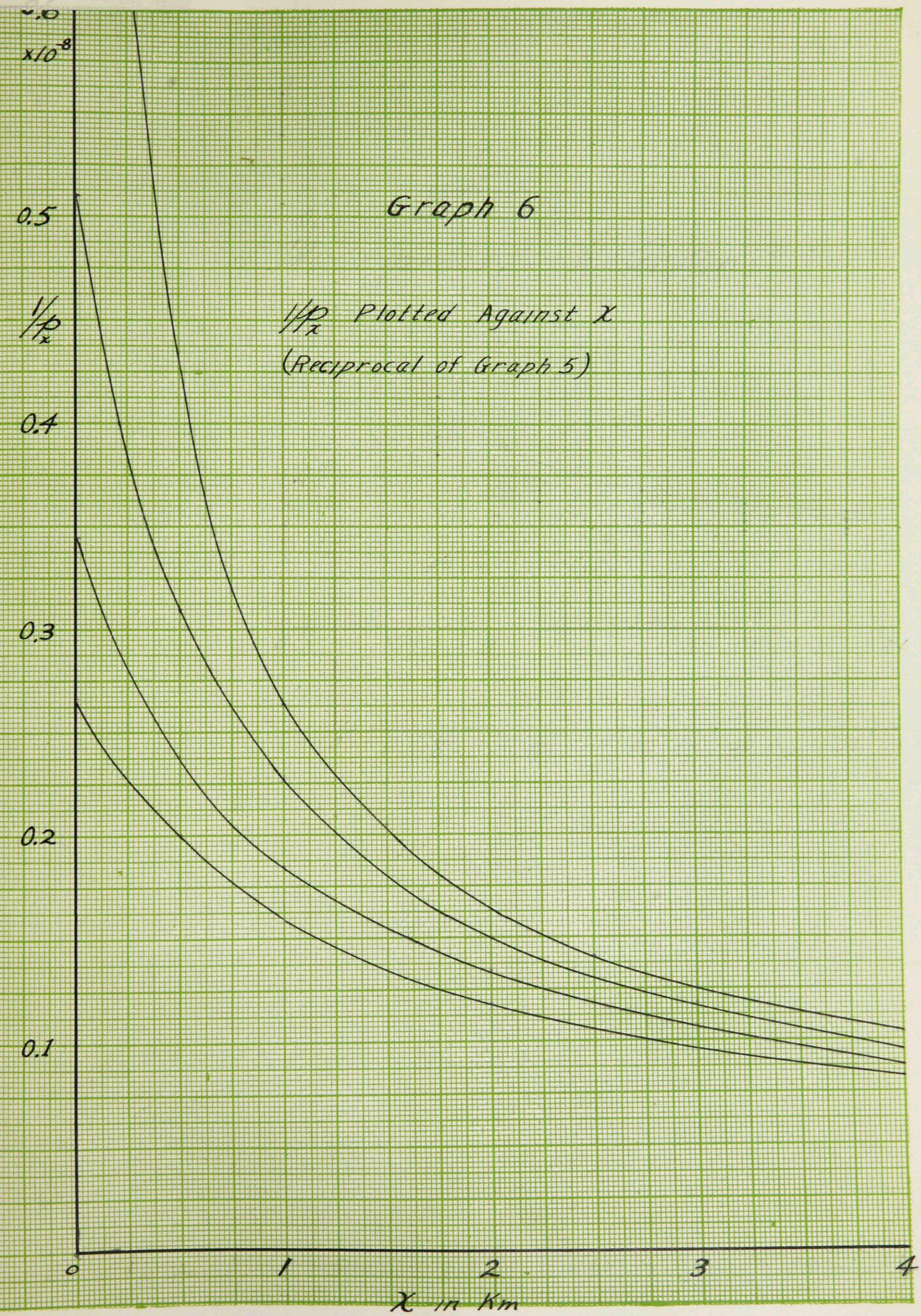

Continuation of Graph 6

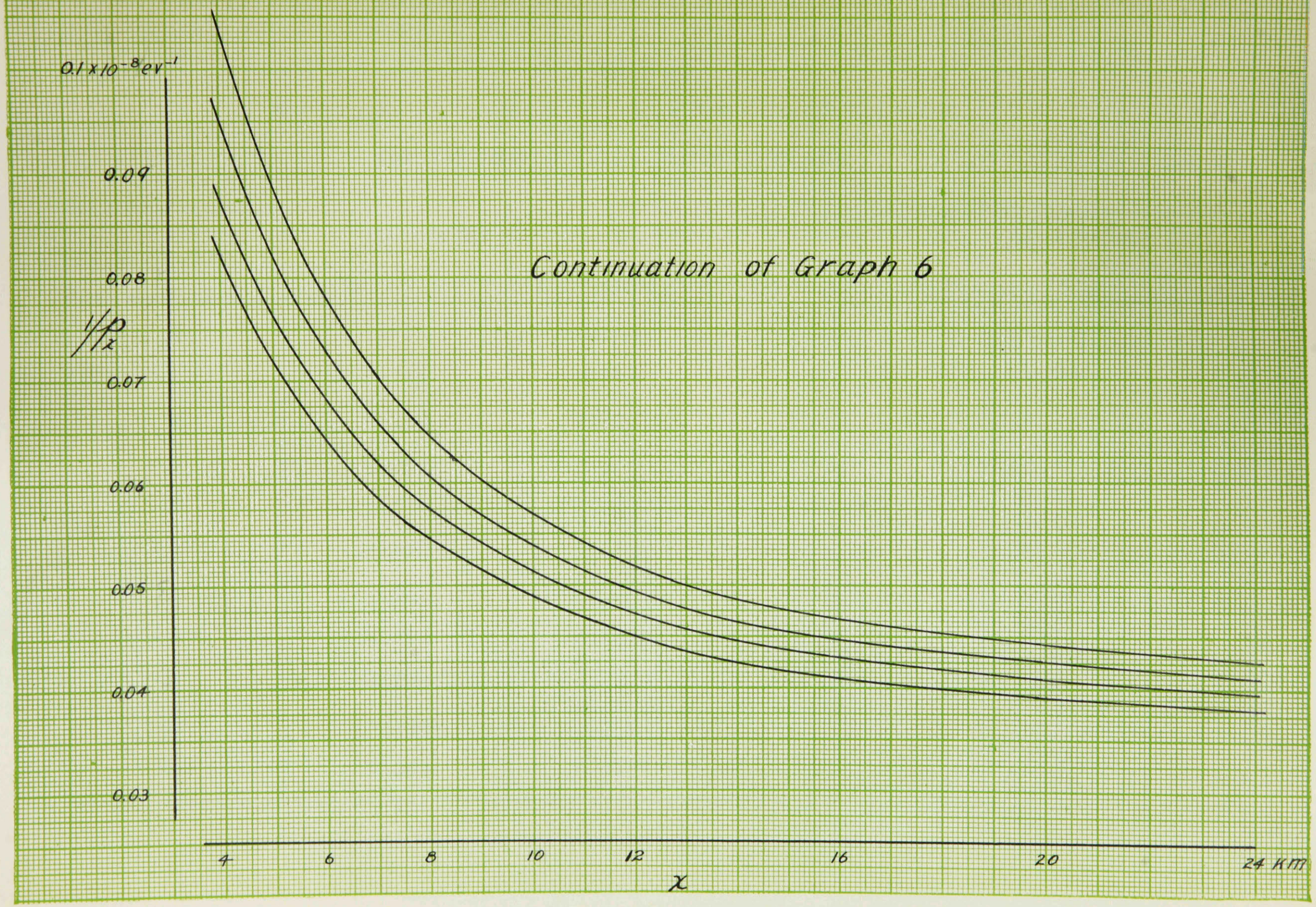

TABLE XI

Reciprocal of Momentum p_x as a Function of Height x

for Different Values of Momentum p_o

x in Km	$1/p_x \times 10^8$ e.v.$^{-1}$ $p_o = 0$	$1/p_x \times 10^8$ e.v.$^{-1}$ $p_o = 1.96 \times 10^8$ e.v.	$1/p_x \times 10^8$ e.v.$^{-1}$ $p_o = 2.9 \times 10^8$ e.v.	$1/p_x \times 10^8$ e.v.$^{-1}$ $p_o = 3.7 \times 10^8$ e.v.
0	∞	0.511	0.345	0.266
1	0.264	0.227	0.185	0.159
2	0.166	0.152	0.133	0.119
3	0.126	0.117	0.105	0.096
4	0.104	0.095	0.0878	0.0824
6	0.0785	0.073	0.0683	0.0641
8	0.065	0.061	0.0577	0.0548
12	0.052	0.0494	0.0472	0.0451
16	0.047	0.0448	0.043	0.041
20	0.0444	0.428	0.0410	0.0392
24	0.043	0.412	0.0397	0.0381

Now equation (3) or (12a) contains the integrand $\int_0^{x'} \frac{dx}{\rho_x}$. This integrand can be evaluated if the area under the curves on Graph 6 is calculated over the region from $x = 0$ to $x = 24$KM. The values of the area for each of the four values of ρ_0 are calculated, and the results are tabulated in TABLE XII.

Since the value of the function for $\rho_0 = o$ is infinite when $\rho_x = o$, The starred value in TABLE XII is approximate. The starred value was obtained in this manner: Values of $\log_e x$ for $x = 0.02$, 0.07, 0.2 and 0.5 KM were plotted against the corresponding values of $1/\rho_x$. These values fitted a straight line which intersected the $1/\rho_x$-axis at $1/\rho_x = 6.25 \times 10^{-8}$. The function for $\rho_x = o$ was then continued to this value of $1/\rho_x$ for $x = o$. Any error in this method would cause an error in the area under the curve between $x = o$ and 0.02 KM. This area is $a = 0.8 \times 10^{-4}$ which is very small compared with the value of the area for $x = o$ to 24 KM. It is not large enough to produce any significant change in the final results. The values of $1/\rho_x$, x, and $\log_e x$ used in this calculation are listed in TABLE XII A.

TABLE XII

Evaluation of $\int_0^x \frac{dx}{\rho_{0x}}$ as a Function of

Height x for Different Values of ρ_0

x in Km	$a \times 10^4$ $\rho_0 = 0$	$a \times 10^4$ $\rho_0 = 1.96 \times 10^8$	$a \times 10^4$ $\rho_0 = 2.9 \times 10^8$	$a \times 10^4$ $\rho_0 = 3.7 \times 10^8$
0 to .22	3.47*			
" .5	4.98	1.97	1.42	1.15
" 1	6.63	3.28	2.46	2.04
" 2	8.70	5.13	4.01	3.40
" 3	10.13	6.45	5.11	4.47
" 4	11.26	7.51	6.17	5.35
" 5	12.21	8.39	6.88	6.11
" 6	13.06	9.16	7.70	6.78
" 7	13.86	9.85	8.35	7.40
" 8	14.48	10.49	8.96	7.97

(Continued)

TABLE XII

(Continued)

X in km	$a \times 10^4$ $p_o = 0$	$a \times 10^4$ $p_o = 1.96 \times 10^8$	$a \times 10^4$ $p_o = 2.9 \times 10^8$	$a \times 10^4$ $p_o = 3.7 \times 10^8$
0 to 9	15.01	11.07	9.52	8.50
" 10	15.70	11.63	10.03	9.00
" 12	16.78	12.65	11.01	9.94
" 14	17.80	13.61	11.93	10.38
" 16	18.73	14.53	12.79	11.65
" 18	19.61	15.45	13.64	12.47
" 20	20.54	16.28	14.46	13.25
" 21	20.98	16.70	14.81	13.74
" 22.5	21.63	17.33	15.44	14.21
" 23	21.86	17.54	14.66	14.42
" 24.0	22.30	17.95	16.07	14.80

Graph 7

$\int_0^{x_1} \frac{dx}{p_x}$ Plotted Against p_x

For (1) $x_1 = 16$ Km

(2) $x_1 = 20$ Km

(3) $x_1 = 22.5$ Km

(4) $x_1 = 24$ Km

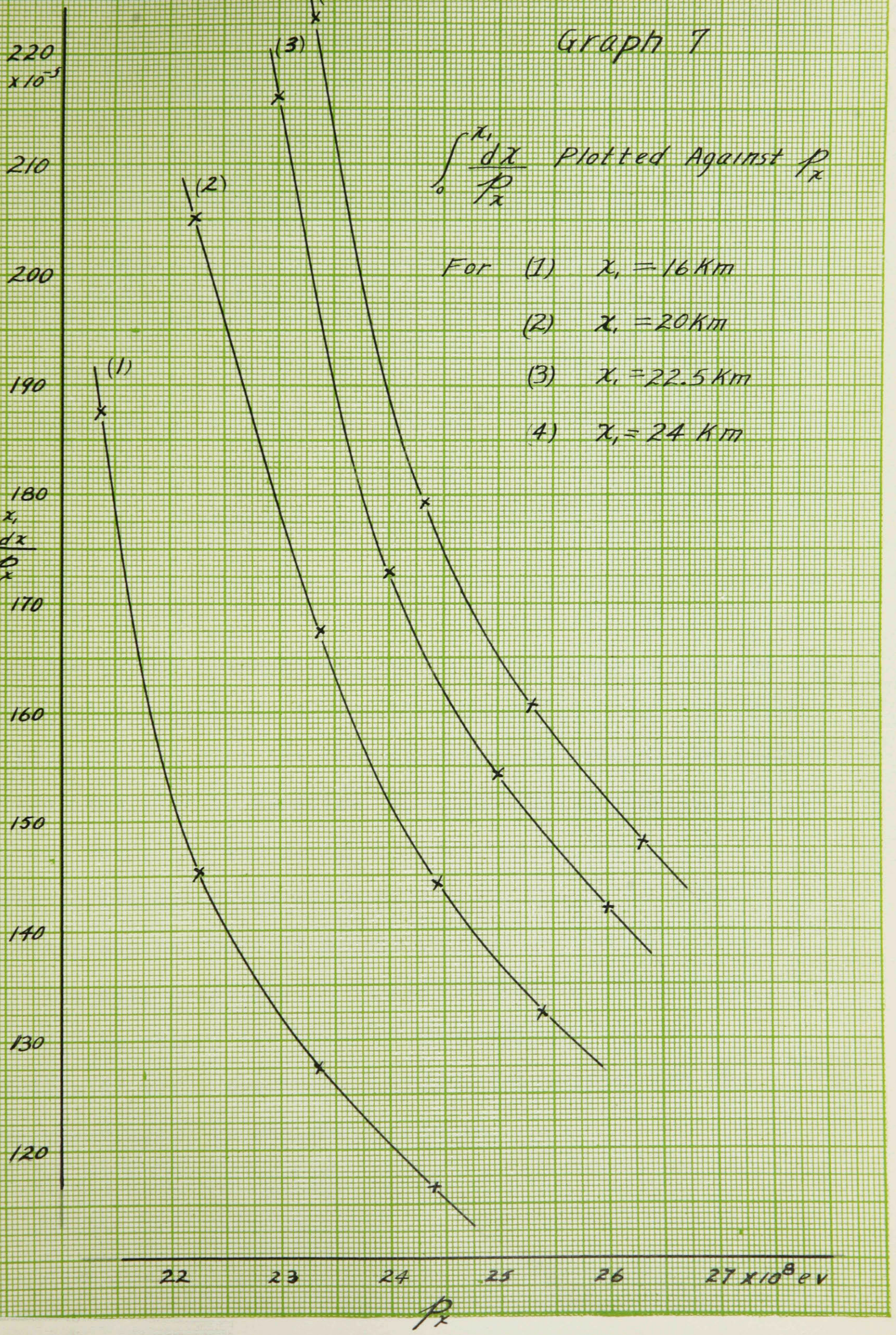

TABLE XII A

Computations Used to Determine The

Starred Value in TABLE XII

$1/p_x$	x	$\log. x$
2.00×10^{-8}	0.02 KM	7.6
1.00 "	0.07 KM	8.85
0.705 "	0.2 KM	9.9
0.414 "	0.5 KM	10.8

Intercept equals 6.25×10^{-8} e.v.$^{-1}$

One of the assumptions made in determining a value of T_0 is the height x_1 of the Mesotron production. In order to try to determine the correct height of origin, the value of the integrand in equation (3) is determined for $x_1 = 16$, 20, 21, 22.5, 23, and 24 KM for the four values of p_0. These values are given in TABLE XII and values of a for $x_1 = 16$, 20, 22.5 and 24 KM are plotted on Graph 7.

The next procedure is to apply equation (9) to Lead in order to obtain the range of Mesotrons in Lead as a function of their momenta. Equation (9) is modified to give the range R in gms./cm.^{2}. It is

$$R_{gms/cm^2} = \frac{\rho m^2 c^4}{2\pi e^4 Z \mu_e N_0} \int_0^{p_x} \left(\frac{p^2}{p^2+\mu^2}\right)^{3/2} \frac{dp}{\log \frac{\mu_e p^3}{200 I^2 Z^2 \mu (\sqrt{p^2+\mu^2}-p)} + \frac{\mu^2}{p^2+\mu^2}} \qquad (9a)$$

Here again the constant terms are evaluated first. They are:

$$\Gamma = \frac{\rho m^2 c^4}{2\pi e^4 Z \mu_e N_0} = 1.64 \times 10^{-6} \text{ for Lead}$$

$$\lambda = \frac{\mu_e}{200 I^2 Z^2 \mu} = 2.04 \times 10^{-11} \text{ for Lead}$$

The equation now becomes

$$R_{gms/cm^2} = \Gamma \int_0^{p_x} \left(\frac{p^2}{p^2+\mu^2}\right)^{3/2} \frac{dp}{\log\left(\frac{\lambda p^3}{\sqrt{p^2+\mu^2}-p}\right) + \frac{\mu^2}{p^2+\mu^2}}$$

The integrand in this equation is evaluated numerically for values of p_x from 0 to 10^9e.v. The values of the integrand for the corresponding values of p_x are tabulated in TABLE XIII. These values are plotted on the lower portion of Graph 3. As in the case for air the area under this curve is calculated for different values of p_x. This evaluation of the area under the curve gives the range in gms./cm.^{2} for Mesotrons as a function of momentum p. The values of range for corresponding values of momentum p are listed in TABLE XIV, and the graph of these values is on Graph 8.

In our experiment we measured range in cms. of Lead so in order to find the corresponding range in cms. in Lead for Mesotrons, the values of range in gms./cm^2 must be divided by the density of Lead (11.35).

TABLE XIII

Calculations Giving The Evaluation of The Integrand

$$P_{Lead} = \Gamma\left(\frac{p^2}{p^2+\mu^2}\right)^{3/2} \frac{1}{\log \frac{\lambda p^3}{\sqrt{p^2+\mu^2}-p} + \frac{\mu^2}{p^2+\mu^2}}$$ as a function of p_x

$p_x \times 10^{-8}$	$\left(\frac{p^2}{p^2+\mu^2}\right)^{3/2}$	$\frac{\mu^2}{p^2+\mu^2}$	$\log \frac{\lambda p^3}{\sqrt{p^2+\mu^2}-p}$	$P_{Lead} \times 10^8$
0	0	1.0	---	0
0.1	.00098	0.991	5.41	0.248
0.2	.0075	0.997	7.57	1.445
0.5	.0895	0.800	10.60	12.9
0.8	0.244	0.620	12.25	32.1
1.0	0.352	0.500	13.10	41.7
2.0	0.716	0.200	15.70	74.1
3.0	0.854	0.100	17.30	80.6
4.0	0.915	0.060	18.42	81.5

(Continued)

TABLE XIII

(Continued)

$p_x \times 10^{-8}$	$\left(\frac{p^2}{p^2+\mu^2}\right)^{3/2}$	$\frac{\mu^2}{p^2+\mu^2}$	$\text{Log}_e \frac{\lambda p^3}{\sqrt{p^2+\mu^2}-p}$	$P_{Lead} \times 10^8$
5.0	0.944	0.039	19.30	80.2
6.0	0.960	0.028	20.10	78.5
7.0	0.970	0.020	20.70	77.0
8.0	0.977	0.0156	21.25	75.6
9.0	0.982	0.012	21.70	74.2
10.0	0.986	0.0099	22.10	73.3

$$\Gamma = \frac{\rho m^2 c^4}{2\pi e^4 n Z \mu_0} = 1.64 \times 10^{-6}$$

$$\lambda = \frac{\mu_0}{200 I^2 Z^2 \mu} = 2.04 \times 10^{-11}$$

TABLE XIV

Range of Mesotrons As a Function of Momentum

$p \times 10^{-8}$	1	2	4	6	8	9
R in gms/cm^2	16	77.95	237.4	397.8	551.8	626.7

Now since we are interested in the range at sea level of Mesotrons which started at a certain momentum, we must plot the momentum p of Mesotrons at height x, as a function of the range in cms. of Lead of Mesotrons with momentum p_o at sea level. This is done in Graph 9. We have four values of momentum p at height x, , and their corresponding values of p_o at sea level. We calculate the range using the values of momentum p_o , and plot it against the four values of momentum p . This procedure is carried out for four values of p, at $x = 16$, 20, 21, 22.5, 23, and 24 KM. The resulting graphs for height $x = 22.5$, 23, and 24 KM are quite linear, while the graphs for $x = 16$, 20, and 21 KM are slightly curved. (The straight line graphs are drawn for only four values of x, , since the others are similiar and lie within the lines drawn...The calculated points lie on the lines only for $x = 22.5$, 23, and 24 KM)

Since these curves on Graph 9 are linear, it indicates

Graph 8

Range in gm/cm² Plotted Against p_x in ev

600 gm/cm²

500

400

R

300

200

100

p_x

1 2 3 4 5 6 7×10^8 ev

Graph 9

26×10^8 ev

25

p_1

24

23

22

(4)

(3)

(2)

(1)

Range in cm of Pb at x_0 Against p_1 at x_1

At (1) $x_1 = 16$ Km

(2) $x_1 = 20$ Km

(3) $x_1 = 22.5$ Km

(4) $x_1 = 24$ Km

R in Pb

0 4 8 12 16 20 24 cm

that the range at sea level is a linear function of the momenta of Mesotrons at the point of origin. From Graph 8 it is clear that the range at sea level does not depend linearly upon their momenta at sea level. Thus the momentum loss in the atmosphere is non-linear to just the extent necessary to cancel the non-linearity shown in Graph 8. This is very convenient, for it means that equal increments in the momentum at the point of origin correspond accurately with equal increments in the sea level range, even though the range is not proportional to the momentum at sea level. Thus, Mesotrons absorbed by each additional centimeter of Lead had equal momentum ranges when produced at some great height, so it is possible to determine the momentum spectrum at this height in this way if we neglect disintegration. The curved relationship in Graph 8 must be used to get the spectrum at sea level. Moreover, as the slopes of the curves in Graph 9 are nearly constant, the momentum range at the origin removed by each additional centimeter of Lead at sea level is 0.156×10^{8} e.v. for all reasonable heights of the Mesotron production layer.

The calculation of the values for Graph 9 finishes the computations. The values of ρ and α listed on pages 25 and 26 were read from the graphs drawn for the calculated values. All integrals in the method were evaluated by plotting the integrands against their variables and determining the areas under the curves by applying Simpson's Rule to the calculated points.

APPENDIX

A suggestion was made on page 29 that the height for the production of Mesotrons is not a definite value, but a variable one depending on the momentum range of the Mesotrons. That is, the Mesotrons arriving at sea level with small momenta were produced at a higher altitude than the more penetrating Mesotrons.

Two recent articles by Hall[16] and Regener[30] seem to confirm this suggestion. Hall performed an experiment on Mount Evans (4.3 KM) very similiar to the one carried out here. He measured the electron and Mesotron intensity for an absorber thickness varying between 1.5 cm. of Lead to 91 cm. In comparing his results with those obtained here, two variations were observed: (1) The maximum in the momentum spectrum for Mesotrons at 4.3 KM was at approximately 6 cm. of Lead absorber, a lower value than that observed here (see Graph 10); and (2) the ratio of the electronic component to the total intensity was less at a particular thickness of absorber than that observed here.

These two variations could be accounted for in this way: The maximum in the momentum spectrum at high altitudes is at a lower value than at sea level because the Mesotrons produced at high altitudes have less momenta than those produced at low altitudes. Hall's experiment could not *detect*

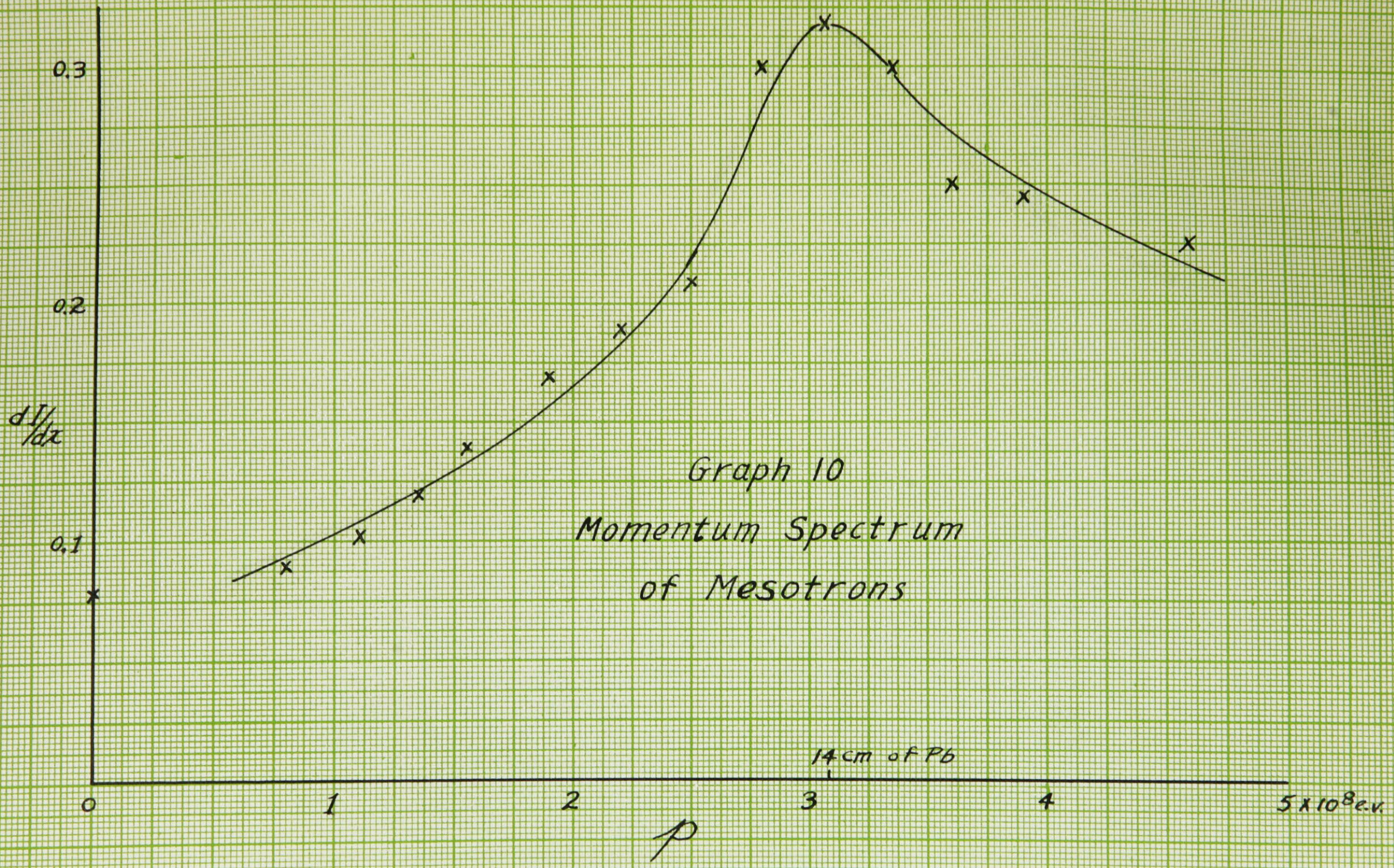

Graph 10

Momentum Spectrum of Mesotrons

all of the more penetrating particles because some of them are produced lower down in the atmosphere, and consequently the maximum was at a lower value. At sea level, the more penetrating Mesotrons will be detected and the maximum is higher. The maximum at sea level would be increased for another reason. The low energy Mesotrons observed at 4.3 KM will have disintegrated before reaching sea level, and hence will be observed as electrons and not as low energy Mesotrons. Here we have a decrease in the low energy Mesotrons due to disintegration and an increase in the high energy Mesotrons due to their being produced nearer the earth. These effects would necessarily shift the maximum in the momentum spectrum to a higher value at sea level.

In support of the suggestion that Mesotrons are produced at low altitudes, we have the results of Regener's experiment. He used a shower counter arrangement designed especially to detect production of penetrating particles. He found evidence that penetrating particles were being produced at low altitudes by non-ionizing radiation.

These results indicate that Mesotrons must be produced by two different processes: The lower energy Mesotrons are produced by protons or high energy electrons at very great heights, while the more energetic Mesotrons are produced all through the atmosphere by photons and neutrons, with the Mesotrons of highest energy being

produced at the lowest altitudes. This is logical since a photon or neutron would have a greater probability of penetrating to greater depths before producing a Mesotron if its energy is greater, and the Mesotron produced would also have more energy.

An additional point to be mentioned in connection with Hall's results is this: The increase in the ratio of the electron component to total intensity at sea level indicates that the number of electrons has been increased due to the disintegration of the low energy Mesotrons detected at 4.3 KM. However, this is true only if the number of shower electrons due to cascade processes remains constant at the two heights. It seems that if the actual numbers of decay electrons could be determined at the two heights, the value of the lifetime τ_0 of the Mesotrons which disintegrate between the two heights could be determined. It is suggested that an experiment designed to determine the number of decay electrons at different heights would be very valuable in the calculation of the rest lifetime of the Mesotron.

BIBLIOGRAPHY

1. Ackemann and Hummel. Naturwissenshaften. 22: 169. 1934.

2. Anderson and Neddermeyer. Physical Review. 50: 263. 1936.

3. Auger, P. Review of Modern Physics. 11: 288. 1939.

4. Auger et. al. Journal de Physique et Radium. 10: 39. 1939.

5. Barnothy and Ferro. Physical Review. 60: 154. 1941.

6. Bhabha. Proceedings of the Royal Society of London. 159: 432. 1937.

7. Bhabha. Proceedings of the Royal Society of London. 164: 257. 1938. 166: 501. 1938.

8. Blackett and Wilson. Proceedings of the Royal Society of London. 165: 209. 1938.

9. Blackett. Proceedings of the Royal Society of London. 165: 11. 1938.

10. Carlson and Oppenheimer. Physical Review. 51: 220. 1937.

11. Clay. Review of Modern Physics. 11: 281-7. 1939.

12. Euler and Heisenberg. Naturwissenshaften. 17: 1. 1938.

13. Evans, R. D. Review of Scientific Instruments. 5: 371. 1934.

14. Exner, F. M. Dynamische Meteorologie. p. 231. Julius Springer, Wien. 1925.

15. Froman and Stearns. Review of Modern Physics. 10: 145. 1938.

16. Hall, D. B. Physical Review. 61: 105. 1942.

17. Heitler. Progress in Physics. 5: 369. 1938

18. Heitler. Quantum Theory of Radiation. Oxford University Press. 1936.

19. Heitler. Proceedings of the Royal Society of London. 161: 261. 1937.

20. Humpherys. Physics of the Air. Fig. 16, Table III. Lippincott. Franklin Institute.

21. Kemmer. Proceedings of the Royal Society of London. 166: 127. 1938.

22. Korff, S. A. Review of Modern Physics. 11: 211. 1939.

23. Maze, R. Journal de Physique et Radium. 9: 162. 1938.

24. Neddermeyer and Anderson. Physical Review. 51: 884. 1937.

25. Neher and Harper. Physical Review. 49: 940. 1936.

26. Neher and Pickering. Physical Review. 53: 316. 1938.

27. Nielsen et. al. Physical Review. 59: 547. 1941.

28. Nishima, Takeuchi and Ichimiya. Physical Review. 52: 1198. 1937.

29. Nordheim. Physical Review. 51: 1110. 1937.

29a. Nordheim. Physical Review. 54: 254. 1938.

30. Regener, V. H. Physical Review. 61: 105. 1942.

31. Rossi. International Conference of Physics, London. 1934.

32. Rossi. Physical Review. 57: 461, 660. 1940

33. Rossi and Hall. Physical Review. 59: 226. 1941.

34. Rossi. Review of Modern Physics. 11: 301. 1939.

35. Ruhlig and Crane. Physical Review. 53:266. 1938.

36. Schmeiser, K. and W. Bothe. Naturwissenshaften. 22: 669. 1937.

37. Schmeiser, K. and W. Bothe. Annelen der Physik. 32: 161. 1938.

38. Street and Stephenson. Physical Review. 52: 1003. 1937.

39. Strong, J. Procedures of Experimental Physics. Prentice-Hall. 1938.

40. Trost, A. Zeitschrift fur Physik. 105: 399. 1937.

41. Wilson, V. C. Review of Modern Physics. 11: 230. 1939.

42. Wilson. Proceedings of the Royal Society of London. 166: 482. 1938.

43. Williams and Pickup. Nature. 141: 684. 1938.

44. Yukawa. Proceedings of the Mathematical and Physical Society of Japan. 17: 48. 1935.

45. Yukawa. Proceedings of the Mathematical and Physical Society of Japan. 19: 1084. 1937.

46. Yukawa. Proceedings of the Mathematical and Physical Society of Japan. 20: 319. 1938.

47. Yukawa. Nature. 143: 761. 1939.